

THESIS FOR THE DEGREE OF MASTER OF SCIENCE

CTH-NT-218

September 2008

In-Core Neutron Noise Analysis for Diagnosis of Fuel Assembly Vibrations

PETTY BERNITT



Nuclear Engineering
Department of Applied Physics
Chalmers University of Technology
S-412 96 Göteborg, Sweden 2008

Abstract

This thesis deals with the analysis of in-core neutron noise measurements in order to diagnose fuel assembly vibrations in the PWR unit R4 of the nuclear power plant Ringhals in Southern Sweden. With the help of noise diagnostic methods the vibrational frequencies of the core and fuel components as well as the axial distribution of the neutron noise, induced by the fuel element vibrations, are determined. After evaluating the obtained auto power spectral density (APSD) plots, the maximum amplitudes of the peaks corresponding to the various vibration frequencies of interest are determined and one can plot their axial distribution. The fundamental vibration mode of the fuel assemblies was found at 1.8 Hz, their second bending mode at 6.8 Hz. The core barrel beam mode vibration has a frequency of 7.8 Hz although the reliability of this interpretation suffers from a lack of information. The shell mode vibration could be found at 19 Hz which is an interesting outcome from an in-core measurement. There were at least two forced vibrations of the fuel assemblies at 9.9 and 10.8 Hz but due to too few measurement data it was not possible to identify the origin of those vibrations in more detail. Furthermore the pump frequency of the primary coolant system could be determined and was found to be 24.9 Hz, i.e. approximately 25 Hz.

CONTENTS

1	Introduction	1
1.1	Nuclear Power	1
1.2	Nuclear Power in Sweden	2
2	General Background	5
2.1	Description of the Problem	5
2.2	Pressurized Water Reactor	6
2.2.1	Reactor Core Internals	7
2.3	Noise	9
2.3.1	Noise Sources in a Nuclear Reactor	10
2.3.2	Zero Power Reactor Noise	11
2.3.3	Power Reactor Noise	12
2.4	Reactor Vibrations	14
2.4.1	Modes of Vibration	17
2.5	In-Core Detectors	19
2.5.1	Fission Chambers	19
2.6	Computational Method and Theoretical Aspects	21
3	In-Core Measurements	25
3.1	Measurement Setup	25
3.2	Technical Data of R4	27
4	Data Analysis and Results	31

4.1	Measurement Data	31
4.2	Power Spectra	33
4.3	Vibrational Frequencies	36
4.4	Axial Amplitude Distribution	38
5	Discussion and Conclusions	41
5.1	Classification of Frequencies	41
5.1.1	The Fundamental Bending Mode - 1.8 Hz	42
5.1.2	The 2nd Order Bending Mode - 6.8 Hz	42
5.1.3	The Beam Mode - 7.8 Hz	42
5.1.4	Unclassified Vibrations - 9.9, 10.8, 12, 15.5 Hz	44
5.1.5	The Shell Mode - 19 Hz	48
5.1.6	The Pump Frequency - 24.9 Hz	48
6	Summary	49
	Acknowledgements	53
	References	57

"Anyone
who expects a source of power
from the transformation of the atom
is talking moonshine."

ERNEST RUTHERFORD
(1871 - 1937)

CHAPTER 1

Introduction

This thesis will investigate the vibrations that occur in an operating nuclear reactor. The measurements needed for this purpose were carried out at one of the pressurized water reactors (PWRs) of the Ringhals power plant close to Varberg, Sweden. Noise diagnostics will be used to analyze the obtained data in order to find the frequencies of the vibrations of the core internals.

This chapter will give a short overview of some few important facts on nuclear power and its status worldwide as well as in Sweden.

1.1 Nuclear Power

There exist several types of nuclear reactors in the world that have the purpose of producing electrical power. At present 441 nuclear power plants operate with the capacity of about 370 GWe, which amounts to about 15% of the electricity need worldwide. If one considers the increasing energy demand of mankind, as well as the fact that fossil fuel supply will be terminated, those numbers will most probably increase in the coming years.

The most common reactor types in operation today are based on light water as reactor coolant and neutron moderator but new units, i.e. different in construction, so-called generation III and IV reactors are being developed on the drawing board as well as in real life and have a significant chance to become the electricity suppliers of the near future. Until then the already existing units have to serve this purpose and in consideration of the high safety standards they have to be checked and upgraded all the time.

1.2 Nuclear Power in Sweden

Regarding pure statistics Sweden takes the first place in the world ranking on "nuclear energy per capita". Table 1.1 is an excerpt from this ranking and shows a few interesting numbers for some of the leading countries regarding nuclear energy.

	MWe/inhabitant	Number of Reactors	Net Output [GWe]
SWEDEN	0.98	10	9
FRANCE	0.97	59	63
FINLAND	0.51	4	5.3
JAPAN	0.38	55	48
USA	0.32	104	97
GERMANY	0.24	17	20

Table 1.1: Excerpt from "Nuclear energy per capita".

The first Swedish reactor, the boiling water reactor (BWR) O1 in Oskarshamn, started operating in 1972 and has a net capacity of 491 MWe. Until 1985 Sweden built 11 additional reactors which can be found along the Swedish coast line.

In 1999 and 2005 the two units in Barsebäck were shut down, c.f. Table 1.2. Nevertheless, Sweden generates about 50% of its electricity with the 10 remaining units, c.f. Figs. 1.1 and 1.2.

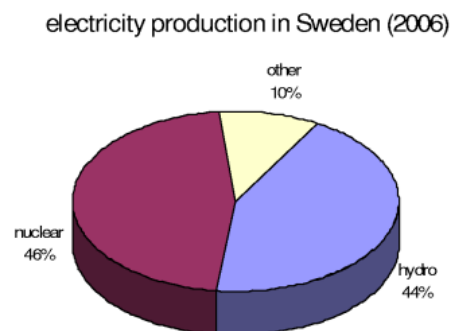


Figure 1.1: Electricity in Sweden is mostly produced in nuclear or hydro power stations.

1.2. Nuclear Power in Sweden

Oskarshamn	BWR O1 (1972) BWR O2 (1974) BWR O3 (1985)
Barsebäck	BWR B1 (1975 - 1999) BWR B2 (1977 - 2005)
Ringhals	BWR R1 (1976) PWR R2 (1975) PWR R3 (1981) PWR R4 (1983)
Forsmark	BWR F1 (1980) BWR F2 (1981) BWR F3 (1985)

Table 1.2: List over the Swedish power reactors.

The Ringhals power plant, which is of special interest in the following work, is owned and run by Vattenfall Sweden AB. With its electricity generation of 3.7 GWe, 20% of Sweden's energy demand, it is both the most productive nuclear facility in Northern Europe and the biggest power plant in Sweden. Furthermore one can claim that Ringhals is one of the biggest nuclear power plants worldwide since it produces about 1% of all the nuclear energy on the planet.

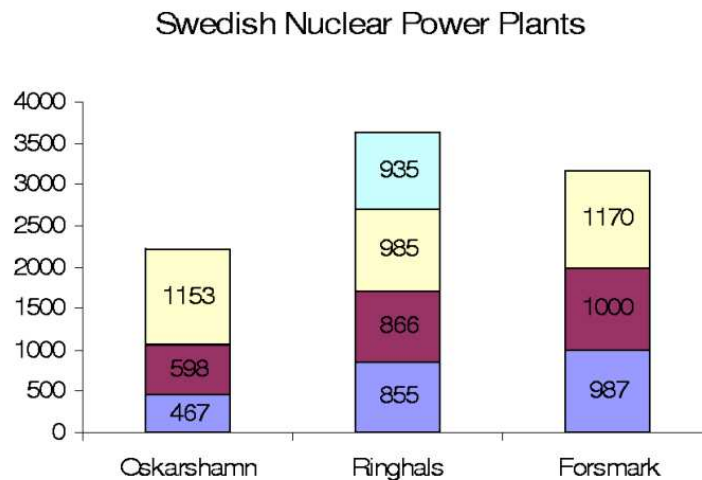


Figure 1.2: Net power in MWe of each Swedish reactor in operation.

Chapter 1. Introduction

CHAPTER 2

General Background

This chapter tries to summarize the knowledge needed to understand the importance and resulting possibilities of neutron noise diagnostics.

First the topics of this thesis are described briefly to get an overview of what was done. Afterwards some basic concepts, which make the framework of this thesis, will be explained in detail.

2.1 Description of the Problem

Due to the construction of a PWR and its core, flow-induced mechanical vibrations can occur, which most likely lead to vibrations of other core internals. Those vibrations are difficult to detect but usually of minor importance for the reactor operation. However, noise diagnostics has the capability to detect them, and hence makes it possible to find normal, i.e. harmless vibrations, and also probable unwanted, anomalous vibrations.

One example of unwanted vibrations can be found in the vibration of single fuel pins which might be due to loose bounds that can even lead to fuel damage, although this kind of event is a rather rare one. It is more common that core vibrations effect the reactor materials such as grids, support plates and surrounding walls. Those parts are constantly exposed to strong radiation which already causes changes in the materials' properties but the additional impacting that follows from the vibrating motion leads, on the long run, to fatigue, wear and even fretting of the core internals.

As long as these kinds of changes in the reactor materials are observed and monitored it is no problem to guarantee the safe operation of a power reactor. One method of doing this is the measurement of neutron noise.

The vibrations that influence the system are very small and do not contribute much to the neutron flux but mathematical tools can help to extract those weak signals in order to obtain detailed information on the reactor internals.

2.2 Pressurized Water Reactor

The aim of this section is to explain how electricity is generated from a microscopic chain reaction so that it finally can reach the customer. Fig. 2.1 is a simplified image of a PWR. It shall help to visualize the following explanation of how a nuclear power station works.

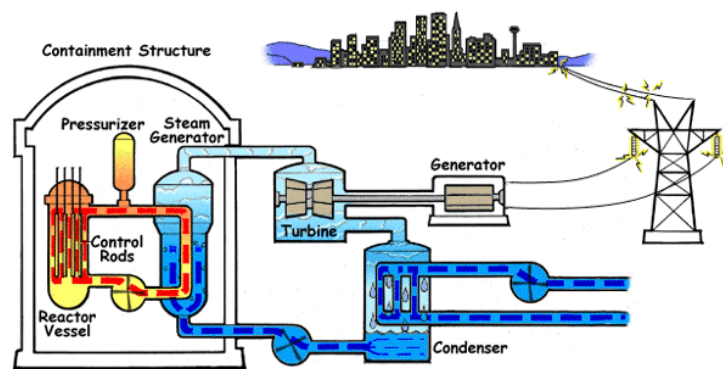


Figure 2.1: Simplified layout of a PWR.

Light water enters the reactor vessel at a temperature of about 280°C . Since boiling inside of the reactor is not allowed, a pressurizer is used to keep the water in the liquid phase. The pressure of this so-called primary coolant loop (reactor coolant system) is around 150 bar. A pump in the bottom of the core forces the water to stream upwards the fuel assemblies where it is heated up to about 310°C - this is less than half the inside-temperature of a fuel pin.

After passing the reactor core, the water is pumped to a system of steam generators. Here is where the secondary coolant loop starts. A steam generator contains light water and works as a heat exchanger - the hot water from the primary coolant loop heats the water inside of the steam generator so that saturated steam at a pressure of circa 65 bar and a temperature of about 280°C is created. The primary coolant cools down and is recirculated

into the reactor vessel. Since the hot steam from the steam generator is wet (saturated) it needs to be dried before passing on to a system of several high and low pressure turbines.

The turbines are connected to an electric generator where electricity is produced ready for delivery to the electric grid. While the steam passes the turbines it turns into a mixture of steam and liquid water which is due to the cooling down and pressure drop that occurs in the turbine system.

This mixture of steam and water is transported to the condenser where the coolant is liquefied so that it can be re-pumped into the high-pressure steam-generator and the cycle can start again.

One very important characteristic of a PWR is that the two coolant loops are separated from each other and contaminated water therefore remains in the reactor vessel whereas in a BWR radioactive steam is directly transported from the reactor vessel to the turbines.

2.2.1 Reactor Core Internals

The heart of a PWR, the reactor core, is a near-cylindrical arrangement of fuel assemblies. Each fuel assembly contains 264 fuel pins (Westinghouse 17x17 design) which are bundled with a number of grids and spacers, and is furthermore equipped with a top and a bottom nozzle. The materials used here are either stainless steel or Zircaloy since these materials only have small cross-sections for the absorption of neutrons. Zircaloy is a metal that contains small amounts of tin (Sn), iron (Fe), chromium (Cr) and nickel (Ni).

The fuel pin is a long tube and is made of stainless steel or Zircaloy. It contains many cylindrical pellets of uranium dioxide UO_2 with a 3-5 % enrichment of the fissile nuclide U-235.

Fig. 2.2 tries to summarize this: in the upper left corner one can see a set of fuel assemblies getting ready for delivery or being loaded in the core. In the subfigure below one finds the layout of a single fuel assembly including the description of some basic parts. Furthermore, one finds an illustration of a fuel pin and a fuel pellet.

Fig. 2.3 shows a horizontal cross section of a single fuel assembly. The grey squares represent the fuel pin positions whereas the white circles symbolize the control rod guide tubes. The orange circle right in the middle is the instrumentation guide tube which cannot really be seen in Fig. 2.2 - more about its function will be explained in the sections below.

Chapter 2. General Background

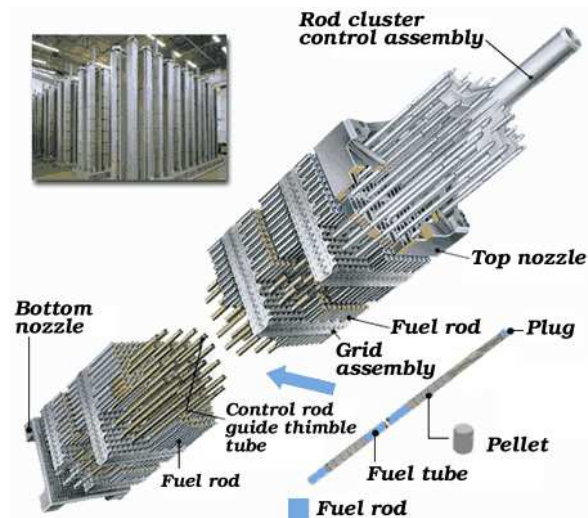


Figure 2.2: The fuel assemblies are lined up, a close look at a single fuel assembly and the fuel pin with pellet.

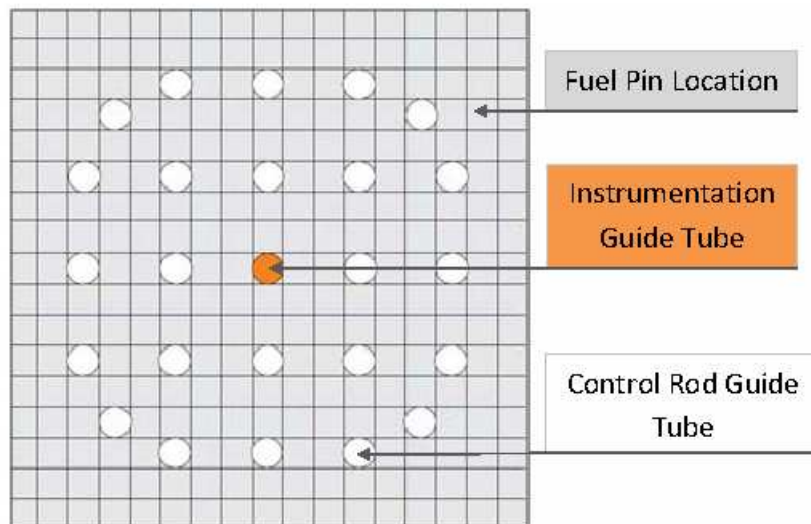


Figure 2.3: Horizontal cross section of a Westinghouse 17x17 fuel assembly.

Finally Fig. 2.4 shows how all fuel assemblies are arranged in the core. In the case of a 15x15 core design one uses 157 fuel assemblies for optimal reactor operation.

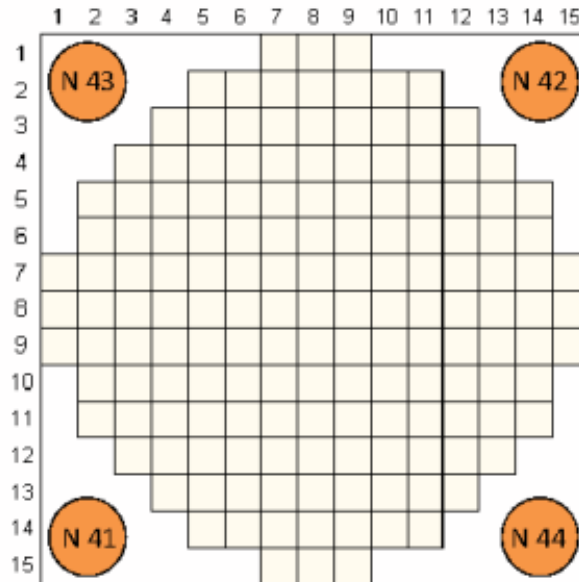


Figure 2.4: Simple image of the Westinghouse 15x15 core layout including the ex-core detectors N41...44.

2.3 Noise

The word noise can stand for a number of different phenomena, especially regarding sound or video applications, so that it is important to state what "noise" means in the special case of reactor operation. Generally one can say that noise is the irregular variation of a measurable variable which changes its characteristics randomly in time. This process can be divided into two categories: stationary and non-stationary noise. Stationary noise remains relatively constant over a long period of time and does not change its character very much whereas non-stationary noise occurs instantly.

In most physical applications noise is regarded as distracting since it makes the determination of the mean value of a variable more difficult.

Chapter 2. General Background

Many methods of experimental and computational nature have been developed to get rid of unwanted background noise in the signals. However, in certain cases, such as noise analysis in reactor cores, the noise, i.e. the fluctuation of the neutron flux, can carry important information that otherwise would get lost in surroundings of strong signals.

A helpful tool that filters out weak and probably informative signals from a dominant signal environment is noise analysis which for example in reactor physics is used to determine basic physical properties as well as technological and dynamical processes. One of the advantageous characteristics of noise analysis is that the system does not need to be disturbed externally because here the fluctuations, that occur completely naturally, are used to determine some of the dynamic relationships between process variables without the need of adding external noise.

2.3.1 Noise Sources in a Nuclear Reactor

The transport of neutrons in an amorphous medium is a random process since many related variables such as neutron flight path, scattering angle and number of neutrons per fission event are also random. As mentioned, in many physical processes the variations around the mean can be neglected. In a multiplying medium, like a reactor, fluctuations should not be neglected since they carry interesting information on several parameters such as reactivity, cross sections and time constants.

The decay of a radioactive substance is an exponential process where the nuclei of the sample decay independently from each other. Hence the different events cannot be correlated to each other and the process itself is said to follow Poisson statistics. Fluctuation measurements become a useful tool when correlations exist between several events and system parameters. Such a case is the development of a neutron chain in a multiplying medium. Here the thermal fission of U-235 causes the nucleus to decay into two fission fragments and 2 or 3 neutrons ($\nu(\text{U-235}) = 2.418$ where ν is the average number of neutrons per fission). Those neutrons slow down while traveling through the moderator and each of them has the possibility to induce further thermal fissions in the fuel. This way a neutron chain develops and all events are time correlated to each other.

There are basically two principles which create correlations between single events and system fluctuations. These two principles lead to noise phenomena which are called zero reactor noise and power reactor noise, respectively.

2.3.2 Zero Power Reactor Noise

Zero power reactor noise describes the neutronic fluctuations in a steady multiplying medium. In such a medium, usually a very low power reactor or critical assembly, all material properties are constant in time, i.e. the materials itself do not fluctuate or vibrate as well as moderator boiling is absent. Hence the reason for the occurrence of the fluctuations lies only in the random nature of neutron transport, c.f. first paragraph of section 2.3.1. The term zero power reactor noise is also based on the assumption that the reactor power is so low that effects on the reactivity due to changes in temperature, pressure or density can be neglected.

Since there are no external perturbations, the dynamic behavior of the neutrons in the reactor is only characterized by the neutron source and the neutron chains, including the correlated processes fission, moderation, absorption and leakage.

In reactor theory this is completely described by neutron kinetic equations such as the forward and backward master equations. Those master equations are based on probability theory and by introducing the zero power reactor transfer function G_0 as a function of frequency, one can plot the neutron noise spectrum for a zero power reactor. A closer look on this will be taken in the following section on power reactor noise, 2.3.3.

One important property of zero power reactor noise is the direct proportionality between the variance and the static mean neutron flux, i.e. the average power.

$$\sigma_Z^2 \sim Z \cdot \left(1 + \epsilon \cdot A \left[1 - \frac{1 - e^{-\alpha t}}{\alpha t} \right] \right) \quad (2.1)$$

Here Z resembles the number of neutrons, i.e. the neutron flux, α and A are constants that describe the neutron decay.

Any deviation from the Poisson variance, which is Λ , gives rise to the correlations that lead to the information "hidden" in a fluctuation measurement like nuclear parameters or criticality.

2.3.3 Power Reactor Noise

The second principle that is associated with correlations between several events and the system's fluctuations is called power reactor noise. The behavior of a power reactor is different from that of a zero power reactor and therefore one has to treat the mechanisms in another way.

In a power reactor neutron flux fluctuations are directly induced by the oscillation of reactor materials like coolant boiling, control rod and core vibrations as well as temperature and density variations of moderator and fuel. Any of those arbitrary oscillations causes the corresponding cross sections to fluctuate randomly and the number of neutrons is instantly affected. Since the cross sections are the determining coefficients in the transport and diffusion equations, the effects of the initial perturbation are carried through the entire process of neutron transport and diffusion.

Power reactor noise can be described by stochastic differential equations where the coefficients are treated as random processes, cf. "cross sections [...] fluctuate randomly". This leads to a randomly distributed time- and space-dependent fluctuation in the neutron flux. One method to extract information on the perturbations that generate noise is called the Langevin technique. This technique neglects zero power reactor noise. As already mentioned before, cf. last paragraph of section 2.3.2, the variance of zero reactor noise is a linear function of the power. The variance of power reactor noise is proportional to the squared mean of the neutron flux so that neglecting zero power noise is justified.

$$APSD_{\delta\phi} = \phi_0^2 APSD_{\rho} |G(\omega)|^2 \quad (2.2)$$

Power reactor noise is widely used in reactor or neutron noise diagnostics since it is possible to observe changes in the noise which in turn might indicate anomalies in the system.

Around 1950 scientists started to use signals from neutron detectors for measuring reactor kinetics and dynamics. Applying a sufficiently high sampling rate and knowing the frequency dependence of the neutron flux, cf. equations 2.3 and 2.2, make it possible to calculate the auto power spectral density (APSD) via fast Fourier transform (FFT).

A simple example for this can be seen in fig. 2.5 which was obtained from measurements at the High Flux Isotope Reactor (HFIR) at the Oak Ridge National Laboratory (ORNL) in the USA.

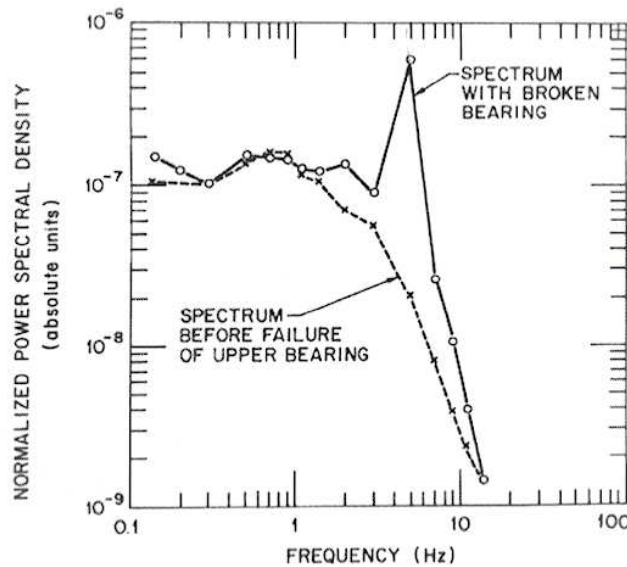


Figure 2.5: NPSD of neutron noise at HFIR before and after control rod bearing break.

The undisturbed system is characterized by the crosses in Fig. 2.5 whereas the dotted curve shows the effect of a perturbation. The peak that occurs at approximately 5 Hz is caused by anomalous vibrations since one of the control rod bearings broke during the measurements.

This event shows clearly that neutron noise measurements can be used to detect probable irregularities and changes in the reactor's behavior. More techniques regarding noise analysis have been developed ever since and are widely used in reactor operation because they improve reactor safety.

The transfer function G_0 that is introduced here describes the undisturbed system and arises from the theory on zero reactor noise. Equation 2.3 is a simplified version of the formula given by Thie (1981, pg. 92):

$$G_0(\omega) = \frac{1}{i\omega \cdot \left(\Lambda + \frac{\beta}{i\omega + \lambda} \right)} \quad (2.3)$$

Fig. 2.6 is the graphical interpretation of equation 2.3 and shows the neutron noise spectrum for an undisturbed zero power reactor. It furthermore can be compared with the crossed curve in Fig. 2.5 and helps to imagine what happens to the spectrum when external perturbations act on the system.

Chapter 2. General Background

Power reactor noise becomes especially interesting in the so-called “plateau-region” which lies between 0.1 and 100 rad/s, where the amplitude of the neutron physical transfer of the reactor is constant, since periodic movements are mostly observed here.

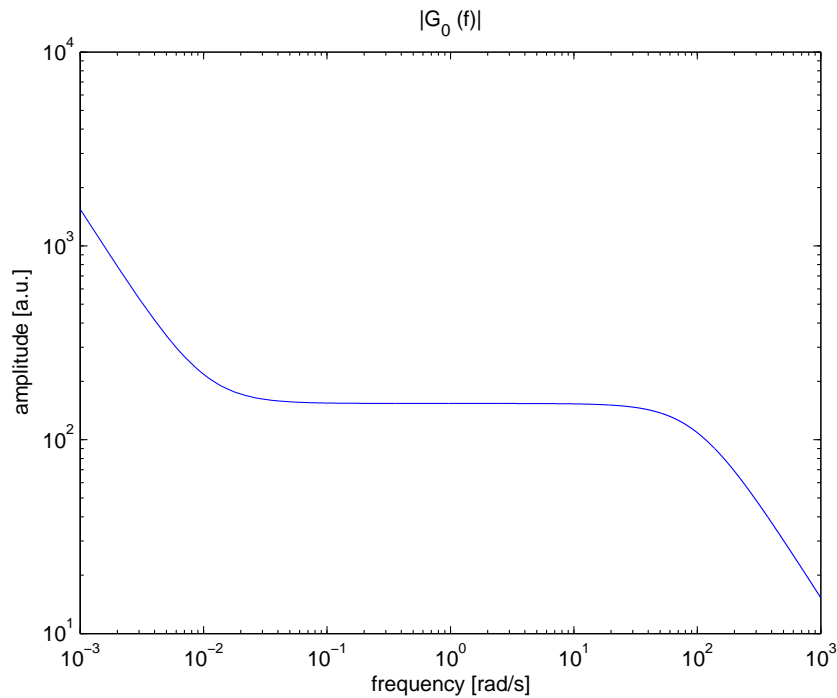


Figure 2.6: Frequency dependence of the amplitude of the neutron noise spectrum for a U-235 zero power reactor with a neutron lifetime of 0.1 ms.

2.4 Reactor Vibrations

This section tries to explain how vibrations in a PWR are generated, such that the need for power reactor noise measurements as a tool for reactor diagnostics is understood. Besides noise that occurs because of reactivity effects or other primary processes, one finds vibrations as a noise source in a PWR.

2.4. Reactor Vibrations

As one could see in Fig. 2.1 the containment building encloses the reactor vessel, steam generators and the pressurizer. Fig. 2.7a shows how those elements are connected with each other and Fig. 2.7b makes clear that the reactor vessel is more or less held up by the junctions of pressurizer and steam generators. One concludes now that the reactor vessel is an object that is only fixed in the top so that it is able to move in a random and even pendulum-like manner.

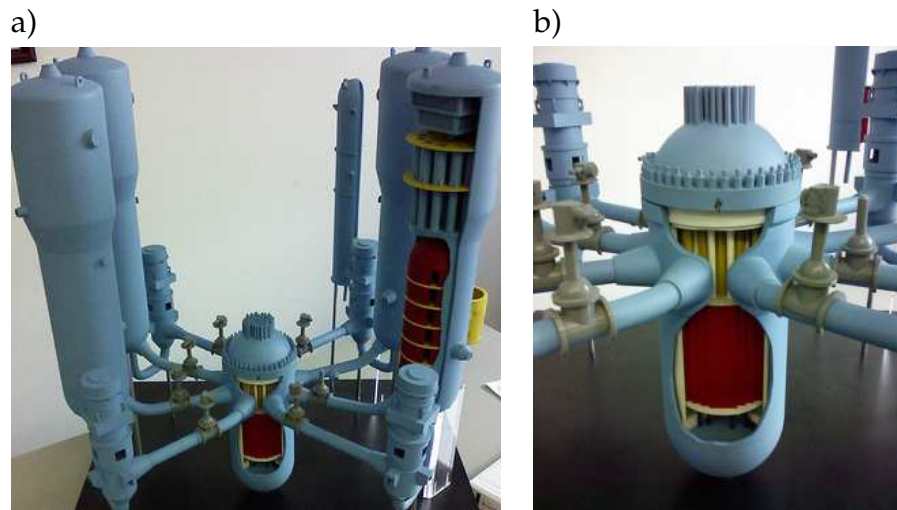


Figure 2.7: This model shows the setup of a Westinghouse PWR. In a) one sees how the different components in the containment building are connected. b) is a magnification of a) in order to see the junctions between core, pressurizer and steam generators.

The core barrel is clamped in the top of the reactor vessel and so the vessel's motion causes the barrel itself and its internal parts to move as well. One example for this might be the lateral movement of the lower and upper core support plate since their motions excite fuel elements and control rods, respectively. This might be clearer when looking at Figs. 2.8 and 2.9 that try to show how several core elements are connected with each other.

Furthermore the strong forces that act on the vessel and the core barrel play an important role for the occurrence of vibrations of the reactor internals. The piping between reactor vessel and steam generator, the inlet nozzle, forces the primary coolant to make a 90° turn in order to stream downwards which causes the water to hit the core barrel's outer surface strongly. This impingement and the high hydraulic pressure of the coolant forces the core barrel to move.

Chapter 2. General Background

Another reason for fuel elements to move, in addition to the excitation through core barrel or support plate motion, is the coolant's upward stream to the outlet nozzle. The speed the coolant obtains here is so high that single fuel elements start to vibrate slightly even if they are fixed in several axial positions.

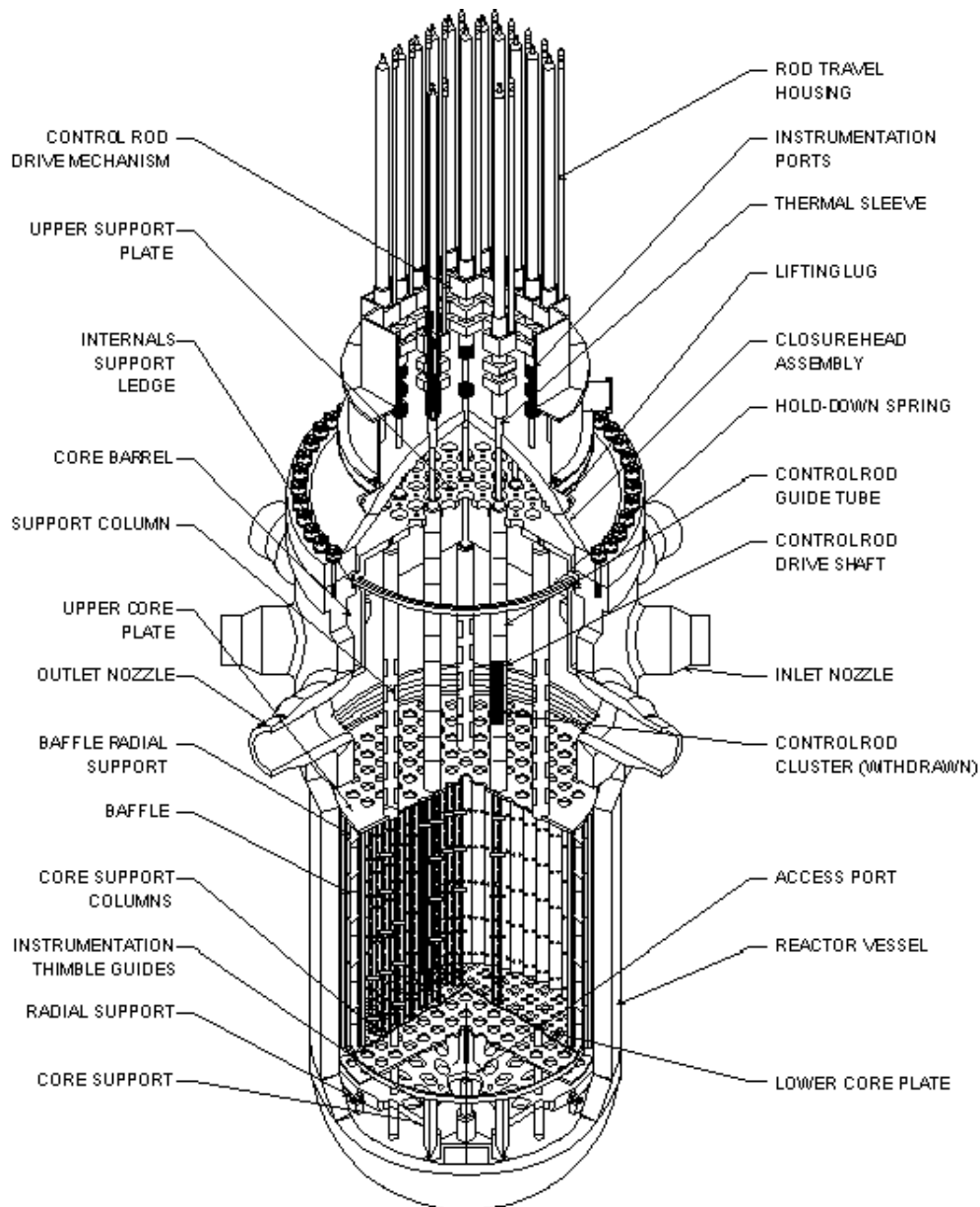


Figure 2.8: Construction drawing of the Westinghouse PWR reactor vessel including labels on several parts.

2.4. Reactor Vibrations

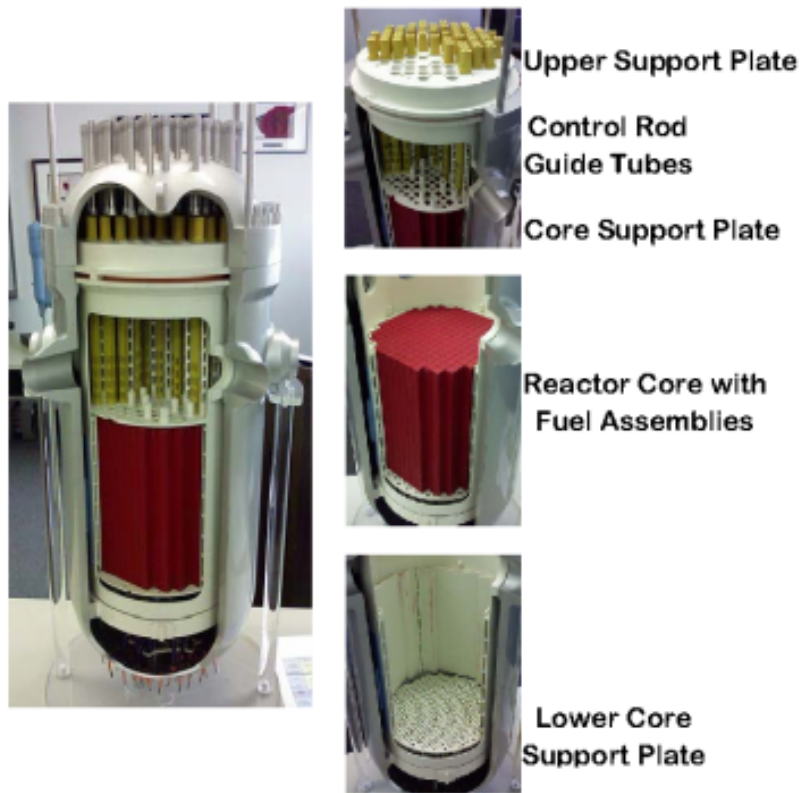


Figure 2.9: Model of the Westinghouse PWR reactor vessel with the core barrel hosting support plates, fuel assemblies and control rods.

2.4.1 Modes of Vibration

The most obvious mode of vibration is the reactor vessel's pendular movement, also known as beam mode vibration. The frequency of this vibration usually lies around 8 Hz whereas another mode of vibration, the shell mode vibration, occurs at about 20 Hz. Those two kinds of core barrel vibrations can easily be recorded by neutron detectors that are positioned outside of the reactor vessel, so-called ex-core detectors. The R4 reactor has 8 of those detectors, 4 positioned in the top and 4 positioned in the bottom, to record the external neutron flux, see also Fig. 2.2b.

As already explained in the introduction of this section, "outer" vibrations influence the "inner" life of the reactor vessel and most likely propagate to the core barrel and its internals where for example fuel rod vibrations might develop.

Chapter 2. General Background

Single fuel rods have the chance to vibrate at the frequencies mentioned above, i.e. at their eigenfrequencies, or to evolve vibrations at completely different frequencies, which correspond to resonances of the driving force. The latter kind of fuel rod vibrations can usually not be measured by the ex-core detectors since their contribution to the total neutron flux might be too small. Therefore one uses detectors inside of the core barrel so that localized fluctuations have a chance to be found. Fuel vibrations are usually considered as a combination of local fuel rod movements and global core movements. Hence, recording in-core noise on a regular basis is one possibility to detect construction defects within the core, as for example a weakly fixed or even loose fuel pin.

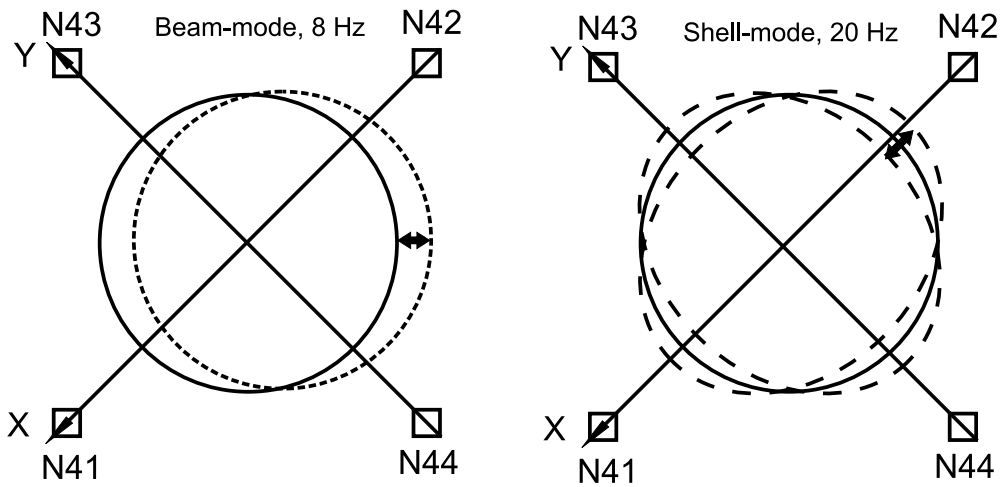


Figure 2.10: Simplified illustration of the dominating core barrel vibration modes, beam and shell mode.

2.5 In-Core Detectors

Controlling a power reactor and assuring the fulfilment of high safety demands requires a number of measurements regarding temperature and pressure, neutron flux, radiation and power level, coolant flow and many more. The essential reaction in a PWR, the fission, is induced by thermal neutrons which is why nuclear sensors have to be based on detectors that mostly respond to low-energy neutrons and, furthermore, are very resistant to radiation damage.

There are two categories of nuclear sensors in order to measure the neutron flux: in-core and ex-core detectors.

As already mentioned before, ex-core detectors are situated outside of the reactor core and simply measure the flux of neutrons that leak out of the core. In a PWR one finds a number of fix ex-core detectors which are placed in the top and bottom of the reactor. Fig. 2.4 indicates their approximate positions.

In-core detectors on the other hand are located in narrow detector-guide tubes in the middle of a fuel assembly, cf. Fig. 2.2, where detailed knowledge on the flux shape can be provided since local variations of the neutron flux might be found. In-core detectors are equipped with a drive mechanism so that they can be moved vertically in the tube they are positioned in with the aim of measuring axial flux distributions. Considering the limited space inside of the fuel assembly, in-core detectors have to be very small - their diameter is in the range of 10mm.

2.5.1 Fission Chambers

The detectors used in the in-core neutron noise measurement at R4 are miniaturized fission chambers. Fission chambers or fission counters are gas counters which are coated interiorly with a fissile isotope in order to measure the number of neutrons arriving at the detector. A common filling gas for the chamber is argon Ar. Its pressure shall make sure that the range of the emitted fission fragments does not exceed the dimensions of the detector. When a neutron hits the coating, fission takes place and the resulting fission fragments move apart from each other. On their way through the counter ion-pairs will be created in the gas since the ionizing density of the fission fragments is very high. Due to the electric field which is applied to the counter, the ion-pairs will drift to the electrodes where they generate an

Chapter 2. General Background

electric pulse. This signal is directly related to the fission rate which in turn is proportional to the neutron flux.

In order to make the fission chamber work properly, it is of particular importance to know the dependence between the coating material and the neutron energy. The fission cross-section for U-235 is much higher for low-energy (slow) neutrons than it is for high-energy (fast) neutrons and therefore fission of U-235 happens with a much higher probability when the nuclei are hit by thermal neutrons. At higher neutron energies the cross-section for inelastic scattering is higher than the one for fission which makes U-235 "blind" to the much less probable process of fast fission. One conclusion of this is that if U-235 is used in fission chambers, the detection of thermal neutrons is possible. Fig. 2.11 shows the cross sections for absorption, scattering and fission with respect to the neutron energy.

When using U-238 instead of U-235 in a fission chamber, fast neutrons can be counted since U-238 fissions at high neutron energies. Taking for example a mixture of U-235 and U-238 as coating for the fission chamber is one reliable method to measure the thermal as well as the fast neutron flux.

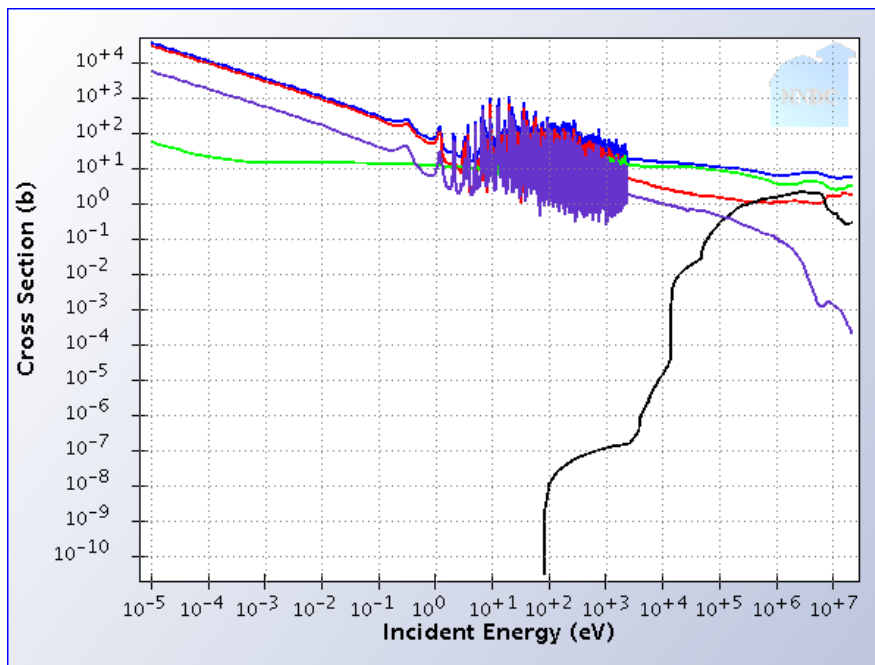


Figure 2.11: Neutron cross sections for U-235 vs. neutron energy. (blue - total; red - fission; green - elastic; black - inelastic; purple - capture)

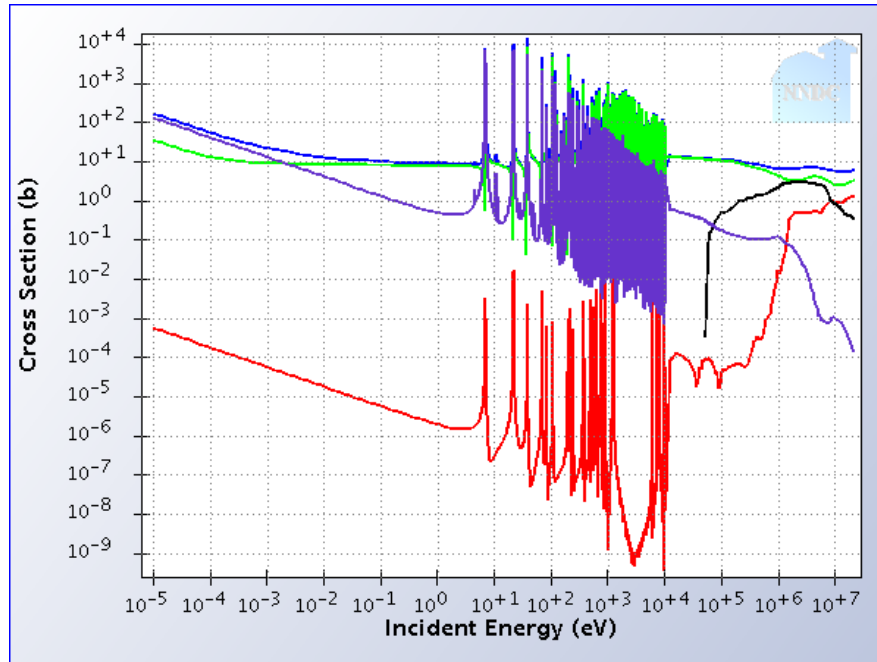


Figure 2.12: Neutron cross sections for U-238 vs. neutron energy. (blue - total; red - fission; green - elastic; black - inelastic; purple - capture)

2.6 Computational Method and Theoretical Aspects

This part of the thesis describes a method for finding the different vibrational frequencies from the measured detector signal. Generally speaking the data taken contains the noise of the system, i.e. a superposition of random processes of different character. In order to obtain information on the noise component of interest, one has to perform spectral analysis, that is to describe the distribution over frequency of the power contained in a signal.

To estimate the auto power spectral density (APSD) in this specific case Welch's method is used: the signal is divided into several segments (blocks) of equal length and the computed periodograms (digital Fourier transforms) - one per segment - are averaged.

The length of a block is determined by the amount of points that will later on be used for the FFT. A window function is applied to each segment in order to generate a filter, "which tapers the ideal impulse response" and in turn results in an increasing resolution of the amplitude.

Chapter 2. General Background

Windowing in this context means to multiply the data sequence in the block with the corresponding values of the window function. The window function used for this specific case is called a Hanning function and is defined as

$$hann(N) = 0.5 \left(1 - \cos \left(\frac{2\pi N}{n-1} \right) \right) \quad N = 0 \dots n-1 \quad (2.4)$$

A graphical interpretation of this can be found in Fig. 2.13.

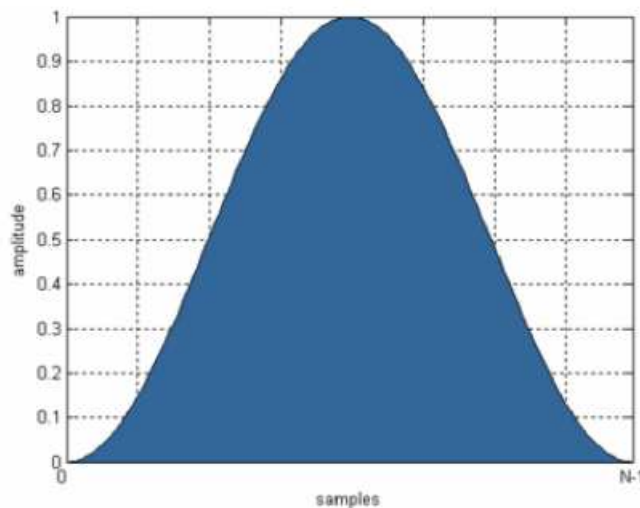


Figure 2.13: The Hanning window.

The windowed data is subsequently put together. It is important to mention that the blocks are used more than once such that each block overlaps with the preceding and consecutive block by 50%. It is easy to see that this enhances the effectiveness of the use of the data.

The periodograms, which are needed for averaging the squared magnitude of the spectral density, are computed by using FFT. Fourier's theorem states that every periodic function of time can be written as a superposition of several sine waves of specified frequency, amplitude and phase and therefore can be transformed into a function of frequency which makes it by means of physics easier to analyse and interpret.

2.6. Computational Method and Theoretical Aspects

A periodic function of time, in this case the measured signal, is expressed in form of a Fourier series:

$$x(t) = \sum_{j=-\infty}^{\infty} X_j \cdot \exp\left[i\frac{2\pi j}{T}t\right] \quad (2.5)$$

Here X_j is the Fourier amplitude at the frequency $\frac{j}{T}$ and can be obtained by:

$$X_j = \frac{1}{T} \int_{-\frac{T}{2}}^{\frac{T}{2}} x(t) \cdot \exp\left[-i\frac{2\pi j}{T}t\right] dt \quad (2.6)$$

Since $x(t)$ is real, the results for X_j , where j is both positive and negative, are related through the condition

$$X_{-j} = X_j^* \quad (2.7)$$

so that all parts of X_j , real and imaginary, are obtained by:

$$\left\{ \begin{array}{l} Re \\ Im \end{array} \right\} X_j = \frac{1}{T} \int_{-\frac{T}{2}}^{\frac{T}{2}} x(t) \cdot \left\{ \begin{array}{l} \cos \\ -\sin \end{array} \right\} \frac{2\pi j}{T} dt \quad (2.8)$$

Expressing equation 2.8 as a sum of $N=T/\Delta t$ makes it transform to

$$\left\{ \begin{array}{l} Re \\ Im \end{array} \right\} X_j = \frac{1}{N} \sum_{k=1}^N x(k \cdot \Delta t) \cdot \left\{ \begin{array}{l} \cos \\ -\sin \end{array} \right\} \frac{2\pi j k}{N} \quad (2.9)$$

and is defined as the FFT. It is important that N is a power of 2 because this condition is the "fast" in FFT.

Now that we transformed the data in the time domain to the frequency domain, it is possible to plot the PSD with respect to frequency in Hz. This will reveal several peaks, some of which can be interpreted as frequencies of vibrations in the reactor core.

Chapter 2. General Background

CHAPTER 3

In-Core Measurements

The in-core neutron noise measurements were performed at the youngest unit of the 4 Ringhals reactors, which is R4. The reason for this decision lies in the outcome of earlier ex-core measurements, which were performed in order to monitor and diagnose the core-barrel vibrations. Such measurements show the beam-mode and shell-mode vibrations as corresponding peaks in the neutron noise spectra. Due to the symmetries of the various modes with respect to the positions of the ex-core detectors, the auto- and cross-spectra, coherence and phase between different detector pairs should obey certain conditions. Further, the auto-spectra of all four ex-core detectors should show a similar shape at the vibration frequencies at the same axial level. However, in earlier measurements deviations from the expected general properties were observed mostly in R4, and to a lesser extent in R3. Hence the hypothesis was set up that in the measurements a combined effect of the core-barrel and the fuel assembly vibrations is observed, which can lend a possible explanation for the irregularities observed in the ex-core detector signals. Thus it was thought that additional in-core measurements might help to answer some of the questions on this problem.

The in-core measurements at R4 were executed on March, 4th in 2008 with the help of Björn Severinsson and Martin Bengtsson.

3.1 Measurement Setup

Five in-core detectors were used to measure the neutron flux at 6 different axial positions such that every detector was kept in each of those axial positions for 15 minutes. After inserting the detectors at the bottom of the core they were firstly moved to the very top of the core and then taken out in several steps. The first axial position was situated 30 cm below the top of

Chapter 3. In-Core Measurements

the reactor core from where each detector was moved in steps of 60 cm until position 6, situated 30 cm above the bottom of the reactor core, was reached. A graphical interpretation of the above can be seen in Figs. 3.1 and 3.2. All in all the in-core measurement took 2 hours.

Furthermore the 8 ex-core detectors, 4 positioned in the bottom and the other 4 in the reactor's top, were used to measure the ex-core noise, although the analysis of this measurement belongs to another project and is not included in the present thesis.

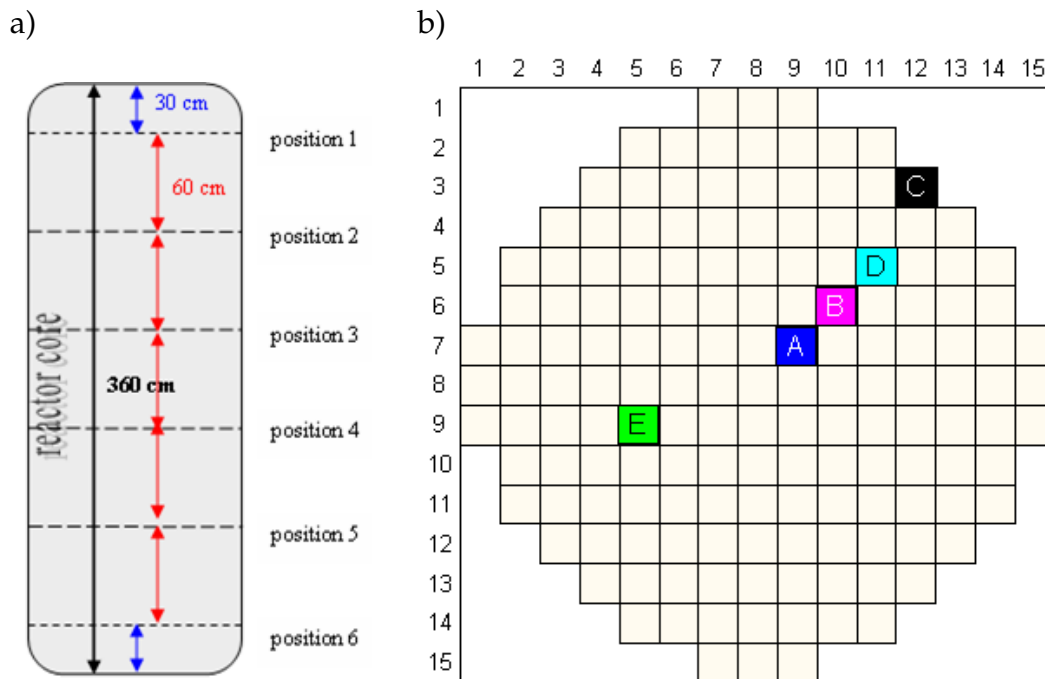


Figure 3.1: a) Axial positions of the in-core detectors. b) Detector positions in the core.



Figure 3.2: This model shows the in-core instrumentation tubes in the bottom of the core where the detectors are inserted.

3.2 Technical Data of R4

The following list summarizes some technical data on the major parts of R4 such as the reactor and vessel, fuel assemblies, control rods, steam generators, turbines and electricity generators.

Reactor Type	PWR
Reactor Supplier	Westinghouse
Thermal Power	2775 MWth
Electric Power	915 MWe
Reactor Vessel	
Weight	330 t
Height	13 m
Diameter	3.99 m

Chapter 3. In-Core Measurements

Primary Coolant Cycle

Number of cooling circuits	3
Operating Pressure	15.5 MPa
Inlet Temperature	284°C
Outlet Temperature	323°C

Secondary Coolant Cycle

Operating Pressure	6 MPa
Steam Temperature	276°C
Steam Flow Rate	1521 kg/s

Fuel Assemblies

Cladding Material	Zircaloy-4
Fuel Weight per Assembly	523 kg UO ₂

Total Number in Core	157
Number of Fuel Pins	264 (17x17 type)

Fuel Pin Length	3.66 m
Fuel Pellet Diameter	0.819 cm

Control Rods

Number	48
--------	----

Steam Generator

Supplier	Westinghouse
Number	3
Steam Flow Rate	507 kg/s

Weight	308 t
Height	20.6 m

Electricity Generator

Supplier	ASEA Stal AB
Number	2
Voltage	21.5 kV
Line Voltage	438.5 kV

3.2. Technical Data of R4

Turbine

Supplier	ASEA Stal AB
Efficiency	32.3%
Speed	3000 rpm
Number of High Pressure Turbines (HPT)	2x1
Steam Temperature before HPT	275°C
Steam Pressure before HPT	5.9 MPa
Steam Temperature after HPT	163°C
Steam Pressure after HPT	0.7 MPa
Number of Low Pressure Turbines (LPT)	2x3
Steam Temperature before LPT	260°C
Steam Pressure before LPT	0.46 MPa
Steam Temperature after LPT	29°C
Steam Pressure after LPT	0.004 MPa

Chapter 3. In-Core Measurements

CHAPTER 4

Data Analysis and Results

To analyze the data obtained from the R4 in-core measurement, a short Mat-Lab code was written. Its aim is to show the axial distribution of the auto power spectral density (APSD) at all axial positions for each of the five detectors.

4.1 Measurement Data

The original data file from the Ringhals measurement, "r4exin.c.txt", contains information on both the in-core and ex-core detectors. This txt-file starts with a header of 17 lines that contains some general information on the measurement as for example total measuring time and sampling frequency. It is followed by an array filled with ASCII entries only which represent all detector signals at the different measurement points.

Due to a total measuring time of 10 882.56 s and a sampling frequency f_s of 62.5 Hz the array consists of 680 180 lines. The time increases in steps of 0.016 s ($=1/f_s$).

The number of columns arises from the number of detectors plus one column, the first one, that represents the different measurement points. The columns 2 to 17 now contain the measurement data of the 13 detectors that were used to obtain information on the vibrations of the system:

- column 2...4: DC signal of the upper ex-core detectors N41, N42, and N43
- column 5...9: AC signal of the in-core detectors
- column 10...17: AC signal of all 8 ex-core detectors.

Chapter 4. Data Analysis and Results

All this makes the file quite big with regard to its txt-format. Thus, in order to cut down on calculation time and to avoid confusion with all the different detector signals, a short code called "detectordata.m" was written. This code splits up the original txt-file and creates one mat-file for the time and one for each detector signal. Here it is important to consider that the measuring time for the in-core detectors was about 1 hour shorter than for the ex-core detectors which makes the in-core mat-files just 400 000 lines long.

Since this thesis mostly pays attention to in-core phenomena it will not contain the ex-core measurements, so the data used in the following are based on the shortened measurement files. All complete ex-core data are of course available for further noise diagnostics.

Fig. 4.1 shows what the pure signal of detector A looks like. Thanks to the strong discontinuities in the signal it is possible to determine the times when the detector was moved in the instrumentation guide tube, since changing its axial position adds more noise to the already noisy signal. A magnification of the signal from detector A in one of its axial positions can be seen in Fig. 4.2.

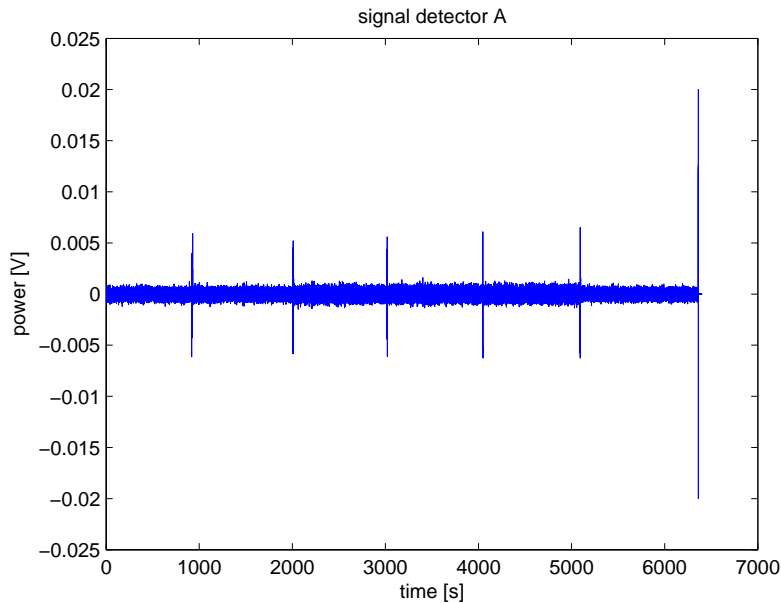


Figure 4.1: Signal of detector A over whole measuring time.

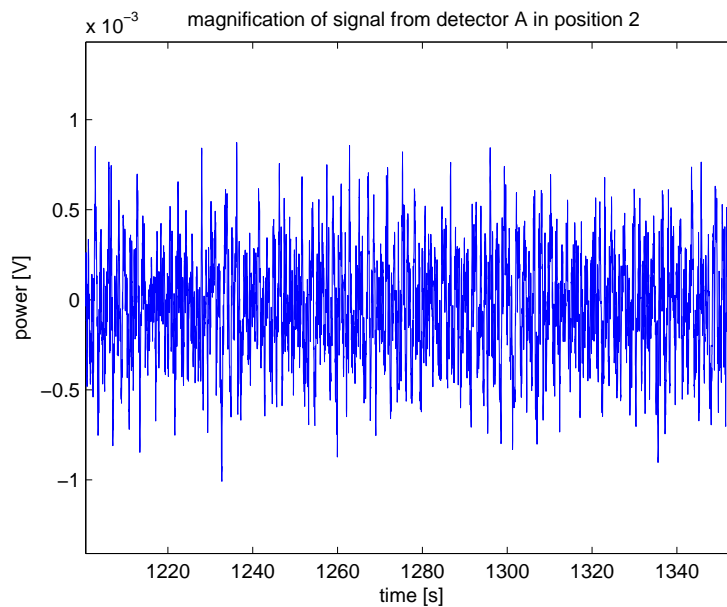


Figure 4.2: Signal of detector A in position 2 scaled up by a factor of 50.

4.2 Power Spectra

By using the 5 mat-files that contain information on the in-core detectors A through E, the auto power spectra for the different detectors and positions are calculated by running the MatLab code named "spetra*.m" which was written for this specific purpose. Here the pre-installed MatLab function "pwelch", named after Welch's method, was used. The algorithm was explained in the previous theoretical part of this work. The output of "spetra*.m" is a set of figures that show the APSD vs. frequency for all measured signals.

The "*" in the program's name stands for the number of FFT points used when calculating the APSD. This number varies between 512, 1024 and 2048 and is a crucial factor for the smoothness of the spectrum. A low but adequate number of FFT points results in a rather smooth curve but causes losses in the precision of the frequency and peak height. A higher number includes more measurement points which results in a noise-like spectrum but at the same time increases the accuracy of the APSD amplitude regarding the reconstruction of the peaks of interest.

Chapter 4. Data Analysis and Results

Therefore a combination of the spectra obtained with 512 and 2048 points was the optimal method to find the different vibrational frequencies and their maximum amplitudes. The "512-version" was used to find a rough estimate of the frequency while the "2048-version" gave the magnitudes used in the further analysis. Figs. 4.3 and 4.4 show the signal for detector A in position 1 with 512 and 2048 FFT points, respectively, and shall help to stress this explanation.

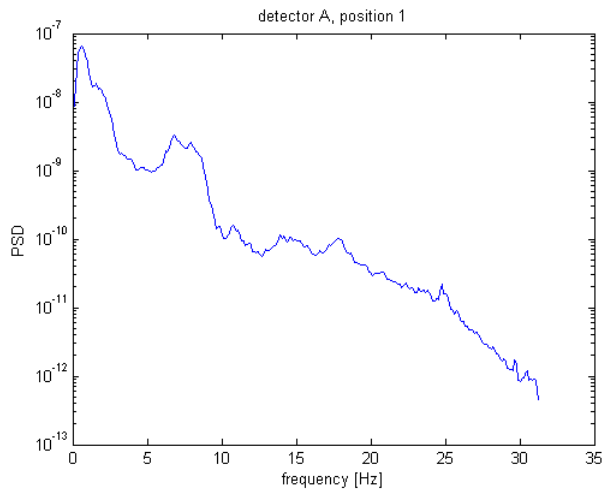


Figure 4.3: APSD vs. frequency when 512 data points per block ("512-version") are used for the FFT procedure.

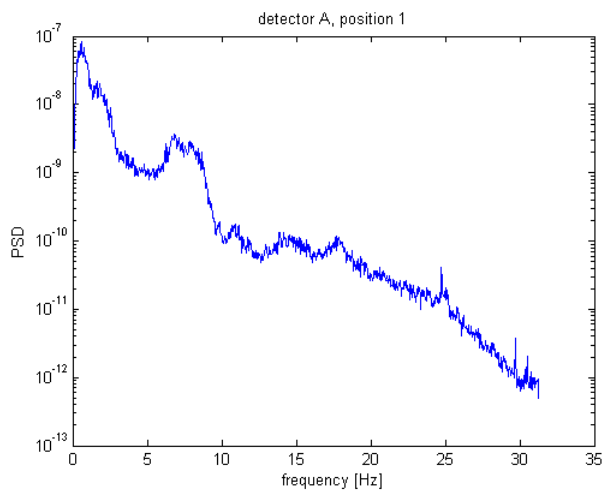


Figure 4.4: APSD vs. frequency when 2048 data points per block ("2048-version") are used for the FFT procedure.

4.2. Power Spectra

As it can be seen in Figs. 4.3 and 4.4, the number of FFT points does not influence the general shape of the APSD spectra. The following figures are going to contain several APSD curves in one plot so that, for the convenience of finding probable similarities or differences between all detector signals, the "512-version" of the spectra will be used.

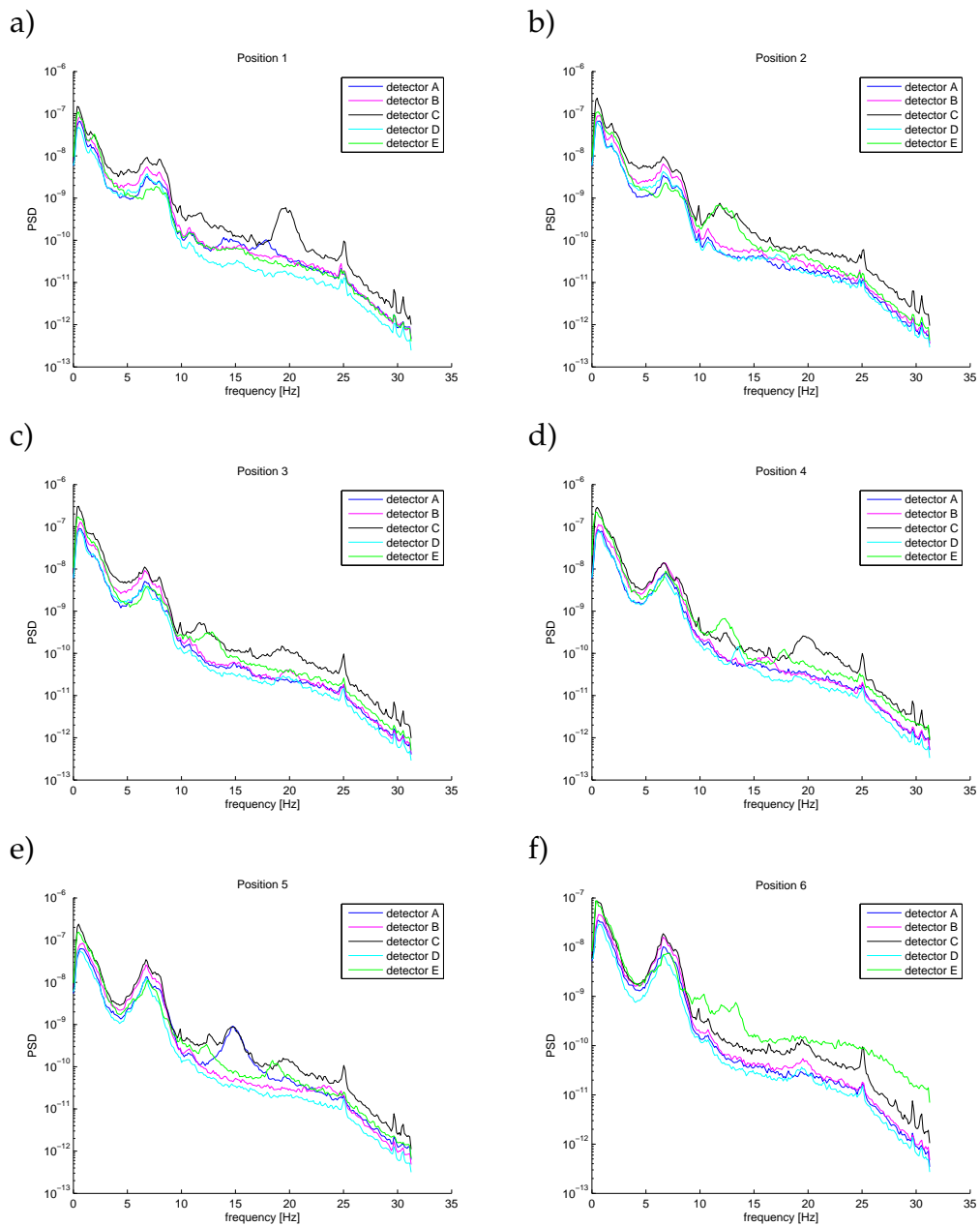


Figure 4.5: APSD vs. frequency of the different detectors for all 6 axial positions.

Each subplot in Fig. 4.5 shows the APSD plots for all 5 detectors in one of the axial positions. Comparing those graphs with each other helps to identify the frequencies of vibration which will be done in the subsequent section. Furthermore the comparison of the graphs might indicate whether the different detectors behave similarly, and generally measure the same phenomenon, or whether some vibrations depend on the detector's insertion position in the core or even on the measurement time.

4.3 Vibrational Frequencies

For the purpose of creating plots that describe the axial behavior of the maximum APSD amplitudes at the vibrational frequencies it is first of all important to find those frequencies.

Comparing Figs. 4.3, 4.4 and 4.5 with the one in section 2.3.2, Fig. 2.6, makes clear that the APSD plots obtained from the measurements follow the general tendency of the zero noise spectrum whereas the obvious peaks in the spectra indicate the frequencies of vibration. First of all the "512-version" of the APSD plots helped to find a rough estimate of the different frequency values. The result from this analysis was then used to determine the "true" frequency values and the amplitude height of the APSD by evaluating the "2048-version" of the 30 processed signals.

The outcome of this is a number of frequencies which occurred in most of the APSD plots. Table 4.1 summarizes the frequencies found as well as the percentage value of their clear appearance. The reason for mentioning how often a peak occurs lies in the fact that it becomes easier to decide whether a peak found at a special frequency can be interpreted as a vibration or not.

Frequency	1.8 Hz	6.7 Hz	7.8 Hz	9.9 Hz	10.8 Hz	24.9 Hz
Fraction in %	50	100	70	70	60	80

Frequency	12 Hz	15.5 Hz	19 Hz
Fraction in %	30	40	40

Table 4.1: Summary over frequencies of vibration.

4.3. Vibrational Frequencies

Due to the high fraction of the peaks found at 6.7, 7.8, 9.9 and 24.9 Hz it is possible to classify those frequencies as vibrational ones.

In 60% of all detector signals one finds a strong peak at 10.8 Hz and in 50% there is a distinct peak at 1.8 Hz. In order to be sure that those frequencies are interesting for the purpose of analyzing core vibrations one has to find out in which spectra those peaks are very low or even missing.

The 10.8 Hz peak is measured by detectors A and B in every position and detector D reveals it in 4 of the 6 positions whereas detectors C and E do not show it clearly at all. Here it is important to point out that detectors C and E measure a high peak at 12 Hz instead, which might interfere with the 10.8 Hz top so that its strength could be weakened and therefore cannot be seen clearly. An important question that arises here is whether it could be possible that the 10.8 Hz is shifted to 12 Hz or whether both frequencies really have to be regarded separately. The conclusions regarding this will be drawn in chapter 5. For the purpose of studying the axial amplitude distribution in section 4.4 it is assumed that the two frequencies are separate from each other.

The peak at 1.8 Hz shows a somewhat different behavior. It is measured by all 5 detectors but only appears really clear in the upper positions. For the remaining positions 4 to 6 one observes that the beginning of each spectrum is broadened which might be due to the 1.8 Hz peak which is contained here and just too weak to be seen in a distinct manner. Furthermore it was observed that, in position 1 only, the frequency always lies slightly below 1.8 Hz, namely at 1.6 Hz. Since exactly this behavior was found numerous times before the measurement discussed here, it is treated as a typical behavior of the vibration at 1.8 Hz.

Even though the top around 19 Hz is only found in 2 out of 5 signals, one can be rather sure that it really is one of the vibrational frequencies of interest. From earlier measurements it is known that the shell mode vibration occurs at approximately 20 Hz. The 19 Hz top was found for every detector in at least one of the axial positions but the fact that it occurred in 5 out of 6 cases for the outermost detector C, is a reliable indicator that this particular frequency represents the shell mode vibration. This mode of vibration reminds on a "fluctuating crunch" of the core, c.f. Fig. 2.10 in chapter 2, and influences the neutron flux strongest on the outside of the core. Since there are almost no changes inside of the core for this type of vibration, ex-core detectors are most sensitive to this vibration mode, but outer in-core detectors could recognize this vibration, too. Detector C is positioned in a fuel assembly which sits on the edge of the core and with regard to the discussion above the shell mode can probably be measured by it.

Furthermore the fuel assembly has less possibilities to move since it is restrained by two core walls and it could be that this limitation is transferred to the detector so that wall vibrations might be recognized.

Even if strong tops were found at 15.5 Hz in 40% of the cases and furthermore every detector measured this frequency at least once, it was not possible to make out any trend behavior regarding their occurrence.

At the end of this section it is maybe important to mention that the phenomena observed, especially regarding the frequencies that only occur with a relatively low fraction, are not very strange to experts in the field of reactor diagnostics. Indeed they have been seen in several earlier measurements but could not be explained in detail yet.

4.4 Axial Amplitude Distribution

With the help of the APSDs calculated and shown above and by classifying the frequencies of interest, bold-marked in Table 4.1, it was possible to generate lists that contain information on the maximum amplitude for each detector and position. In the beginning those tables are of the format "axial*.xls" but later on their entries are transformed to matrices that are saved as mat-files. Finally those files are used as input data for the MatLab code "axial*.m" which plots the axial distribution of the APSDs for all vibrational frequencies identified above.

The 6 resulting plots are summarized in Fig. 4.6. Here each subplot represents one of the vibrational frequencies and shows its maximum amplitude with respect to the reactor height for each detector.

Furthermore it was of interest to follow the amplitude distribution for those frequencies that are difficult to classify. For the purpose of creating plots that hopefully help to prove the assumptions made above or reveal the origin of the peaks that occur at 12, 15.5 and 19 Hz, another MatLab code was written. This short program, named "axialextra.m", works in the same manner as "axial*.m" with the only difference that the vectors that result in the axial amplitude distribution of the chosen frequencies were generated manually. Of course the resolution is not as good as in Fig. 4.6 since the number of peaks that were identified in a definite manner is substantially lower than for the other frequencies. However, comparisons between the different graphs might help to understand the nature of some of the unexplained phenomena anyway.

4.4. Axial Amplitude Distribution

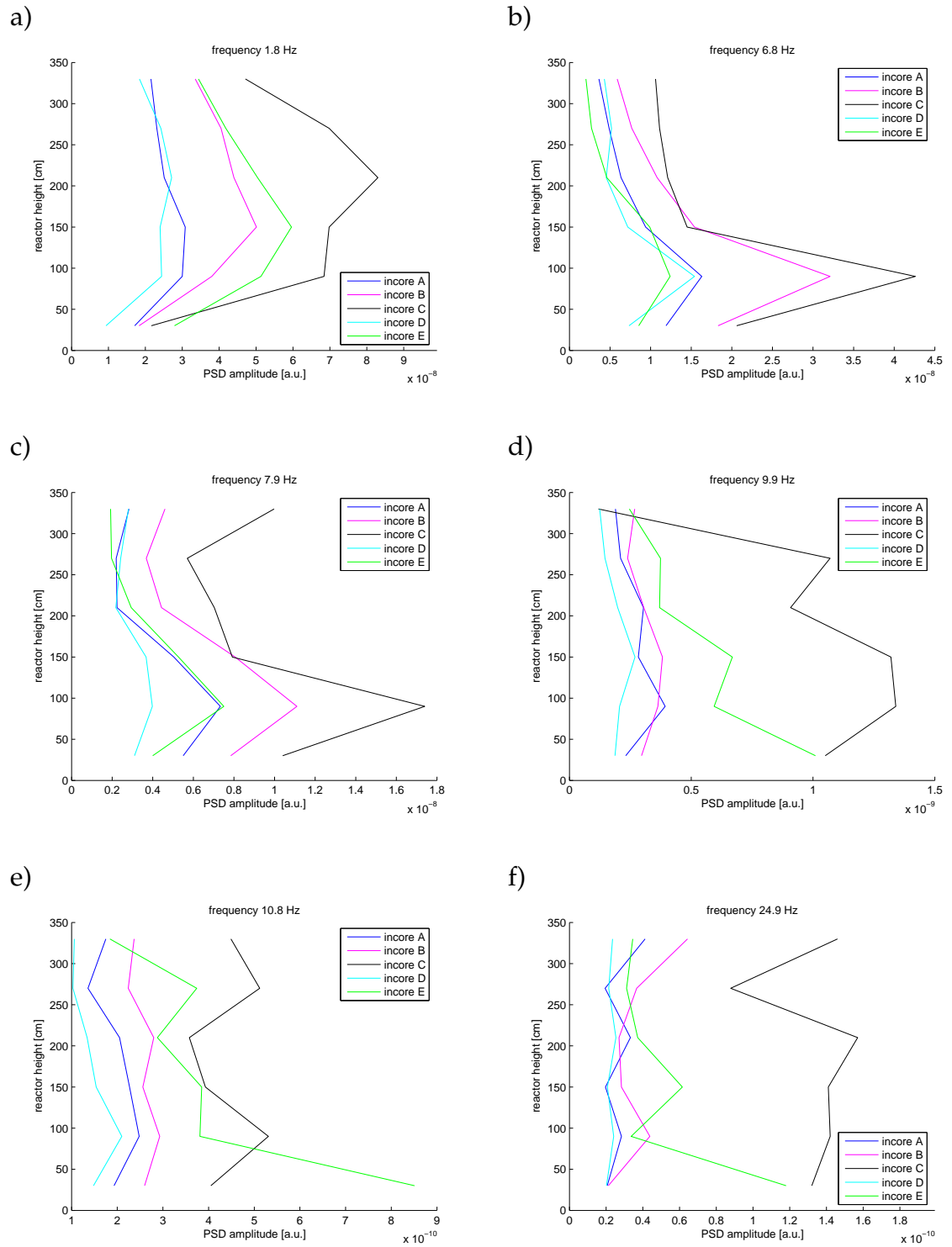


Figure 4.6: Amplitude vs. height for each vibrational frequency.

Chapter 4. Data Analysis and Results

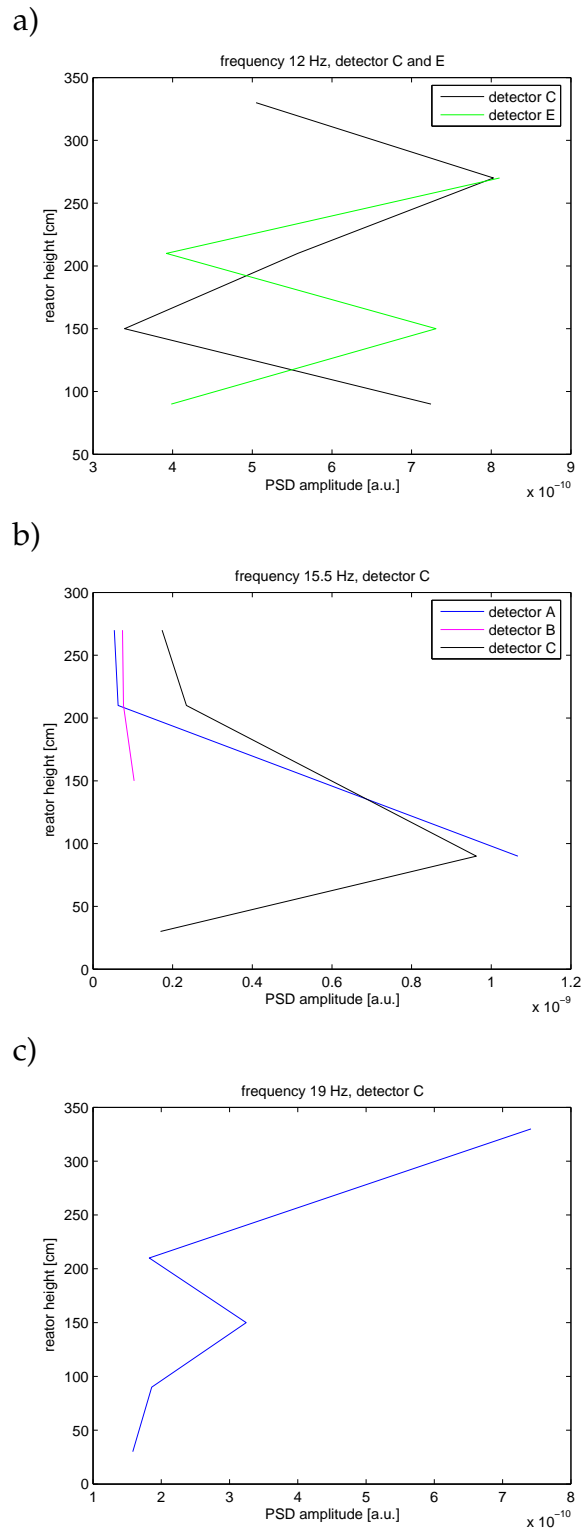


Figure 4.7: Amplitudes vs. height for 12, 15.5 and 19 Hz.

CHAPTER 5

Discussion and Conclusions

The aim of this chapter is to summarize the main results of the measurements and to draw conclusions from the plots obtained in chapter 4. Here the frequencies will be classified regarding their origin and type so that characteristics on the system can be found.

5.1 Classification of Frequencies

Classifying the frequencies by their shape will partly be done by the help of a work on in-core measurements at R4 in 1998 (Demazière et al, 1999) which showed theoretical mode shapes in an abstract manner. The plots that were created in that report are shown in Fig. 5.1 and include the boundary conditions of the occurring vibrations.

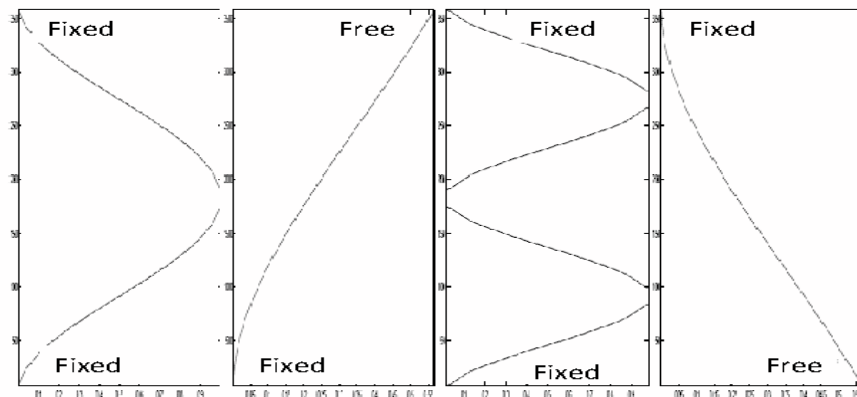


Figure 5.1: Theoretical mode shapes.

5.1.1 The Fundamental Bending Mode - 1.8 Hz

From the literature on earlier in-core measurements it was found that the vibration at 1.8 Hz corresponds to the fundamental, or first order, bending mode vibration of the fuel assembly. Comparing the measured axial amplitude distribution at this frequency in Fig. 4.6a with Fig. 5.1 leads to the insight that the 1.8 Hz vibration has fixed conditions in both ends of the fuel assembly. This makes perfectly sense since the fuel assemblies are in principle attached between the upper and lower core support plate so that their vibrations most likely generate the fundamental fuel assembly vibration at 1.8 Hz.

All 5 in-core detector data show that the APSD amplitude increases to its maximum in the middle of the core and then decreases again to a value slightly smaller than the one in the first axial position.

5.1.2 The 2nd Order Bending Mode - 6.8 Hz

The rather strong vibration at 6.8 Hz is classified as the second order bending mode vibration of the fuel assemblies with fixed conditions in the top and free conditions in the bottom. The amplitude increases much in the lower part of the core which indicates that the vibrations here are stronger than in the upper part of the core. That specific behavior was measured by all 5 detectors whereas the signal from detector C is again dominating.

With regard to the results obtained from vibration measurements at the Sequoyah-1 reactor in 1985 one can conclude that the vibration at 6.8 Hz is a result of the movement of the lower core support plate which is triggered by the pendulum movement of the core barrel.

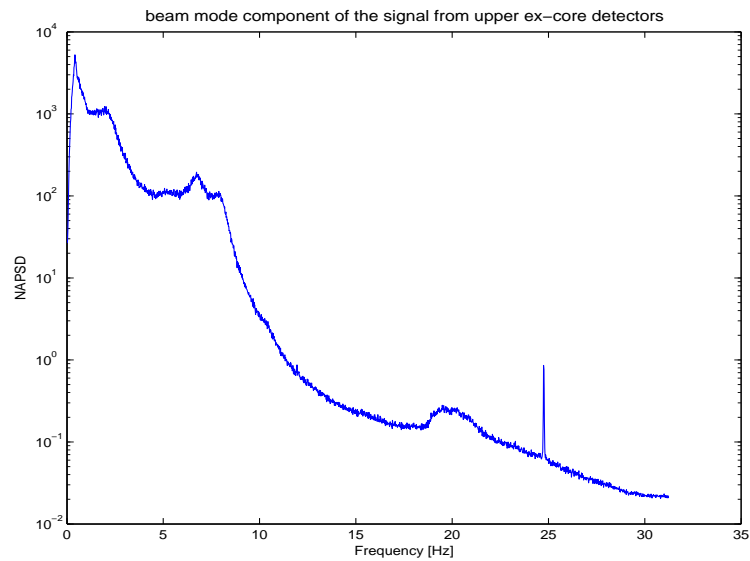
5.1.3 The Beam Mode - 7.8 Hz

The vibration at 7.8 Hz is assumed to originate from the classical beam mode vibration with a fixed end in the top and a free end in the bottom. Even if there is, according to Fig. 5.1, no theoretical mode shape that shows a behavior similar to the experimental one, the vibration is classified as the fuel assemblies following the pendulum movement of the core barrel. Unfortunately there are not many references that stress this interpretation but comparing the in-core with the ex-core spectra might help to prove this assumption.

5.1. Classification of Frequencies

The ex-core measurements used here were made simultaneously with the in-core measurements and the analysis was made by A. Hernandez-Solis at the Department of Nuclear Engineering of Chalmers. Fig. 5.2 shows the NAPSD (Normalized Auto Power Spectral Density) vs. frequency of the beam mode component for the upper and lower ex-core detectors.

a)



b)

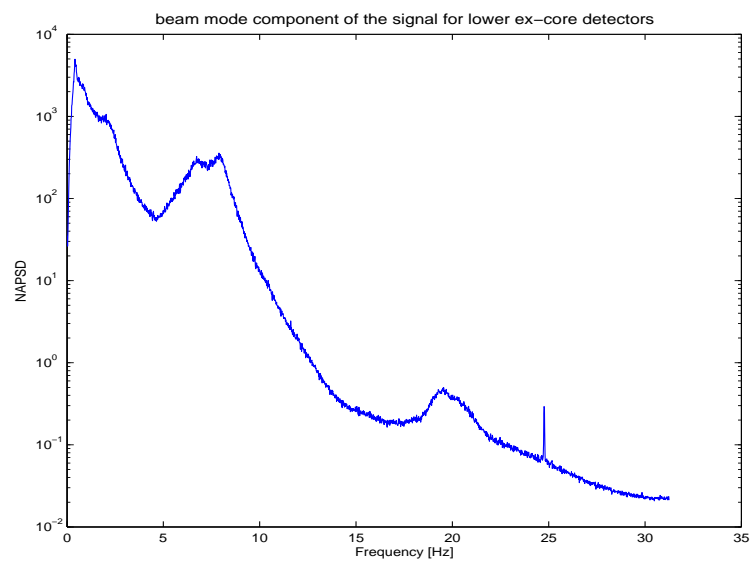


Figure 5.2: NAPSD vs. frequency for the upper and the lower ex-core detectors.

Chapter 5. Discussion and Conclusions

The frequencies of interest in the 6 - 8 Hz region agree almost exactly with the frequencies measured in the in-core measurement. The upper part of the core vibrates at 6.7 and 7.9 Hz, whereas the vibrations found in the lower part are 6.8 and 7.9 Hz. So the double peak that was observed in 70% of the in-core measurements also occurs in the ex-core noise spectra with one important difference. In the case of the in-core spectra the top at 7.8 Hz was always lower than the one at 6.8 Hz. But as one can see in Fig. 5.2, this is only true in the upper half of the core in the ex-core measurements. In the lower part the vibration at 7.9 Hz dominates over the peak at 6.8 Hz, and it is still difficult to determine the "real" frequency of the beam mode vibration.

One fact that is consistent between the in-core and ex-core measurements is that the NAPSD amplitude increases in the lower part of the core and this was also observed in the amplitude shapes of all 5 in-core detectors.

Even if the consideration of the ex-core measurements might be more confusing than enlightening it is suggested that the vibration at 7.8 Hz corresponds to the beam mode since there were at least two more references that stated a frequency around 8 Hz for the beam mode vibration.

An additional comment regarding the double peak in the 6 - 8 Hz region will follow in the summarizing chapter of this thesis since the correct classification of the two peaks is still unclear.

5.1.4 Unclassified Vibrations - 9.9, 10.8, 12, 15.5 Hz

The classification of the vibrations at 9.9, 10.8, 12 and 15.5 Hz is far more complicated than for the other frequencies found. All detectors behave differently, the resolution of the axial amplitude distribution for 12 and 15.5 Hz is not sufficient and references from literature could not be found.

The two last reasons above make it impossible to categorize the 15.5 Hz vibration. By looking at the shape created by detector C one can state that the vibration has fixed end conditions, cf. Fig. 4.7b, but this information is not even enough to prove that the resonance found is a real fuel vibration or just an unexplained perturbation that could result from wall movements. Remember that detector C is the outermost one and due to this might show a behavior different from the other in-core detectors. The observed shape reminds of a higher order vibration mode and could be traced back to wall effects but its definite origin remains unclear so far.

5.1. Classification of Frequencies

In the following the different curves for the 5 detectors in Fig. 4.6d will be discussed. Here one observes that the vibration has fixed conditions in both ends in all cases except for detector E which has fixed conditions in the top and free conditions in the bottom.

The shapes of the curves for detectors B and D remind to some extent of the fundamental mode shape since the maxima of the amplitudes are found in the middle of the reactor but drawing concrete conclusions from this does not appear possible, mostly since the signals of the other detectors behave in a different manner.

The shape for detector C might be interpreted as a higher order vibration mode shape whereas the shape created by detector A could be something like a superposition of C and D. Here the question appears whether it is possible that the different in-core detectors can actually measure the individual behavior of the fuel assembly they are placed in so that one is able to find details on the vibrations of a single fuel assembly.

At last the shape of detector E is similar to the theoretical one that represents the beam mode. Hence one reasonable argument here could be that it resembles the probable swinging movement of the fuel assembly in core position L9. It might also be of interest that the shape of detector E behaves in exactly the same way as for the 10.8 Hz resonance, cf. Fig. 4.6e. It is almost unfortunate that the amplitude for detector E in the case of the 12 Hz resonance misses measurement points in the uppermost and lowest axial position and therefore makes the resolution of Fig. 4.7a poor. This makes it difficult to state that the frequency at 10.8 Hz is really shifted to 12 Hz. Assuming now that the vibration of a fuel assembly might be due to a loose fixing in the lower core support plate remains unjustified. Fig. 5.3 is a comparison of the axial amplitude distributions for detector E at the resonances at 9.9, 10.8 and 12 Hz and shall help to stress the statements made above.

Chapter 5. Discussion and Conclusions

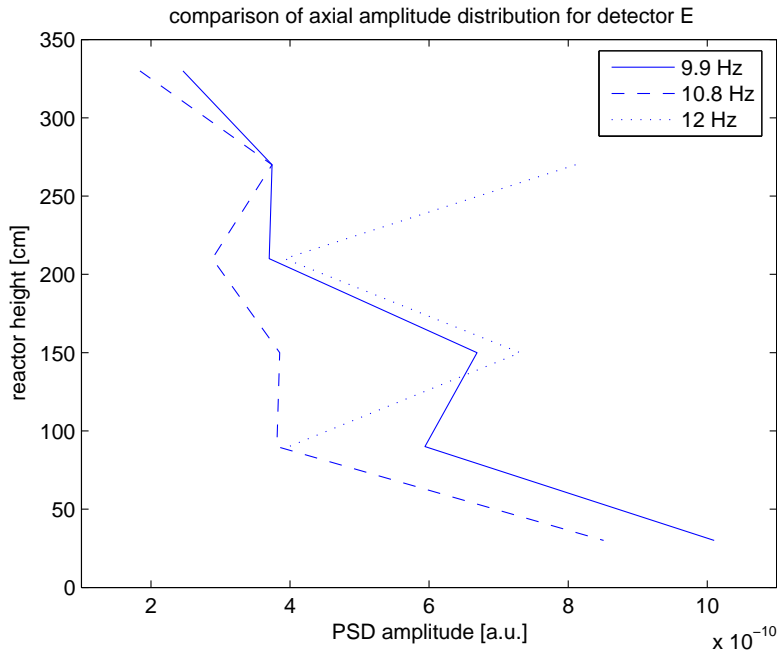


Figure 5.3: Comparison of the mode shapes for detector E in the range of 10 - 12 Hz.

Analyzing Fig. 4.6e in the same manner as Fig. 4.6d does not lead to better insights. The amplitudes for detector A in both figures behave in principle alike as it can be seen in Fig. 5.4a. However, classifying this vibration as a fundamental one seems unreasonable. One could interpret the resonances at 9.9 and 10.8 Hz as forced first order vibrations, again with fixed end conditions, of the fuel assembly in core position G7 caused by outer vibrations or by the coolant flow.

The shape for the vibration at 10.8 Hz for detector B reminds of a second order vibration with fixed end conditions. Due to the fact that the shapes for 9.9 and 10.8 Hz do not look similar, cf. Fig. 5.4b, it is assumed that these two frequencies represent two different vibrations. The one at 9.9 Hz predicts a strong vibration due to the lateral movement of the lower core support plate which particularly acts on the fuel assembly in core position F6, whereas the resonance at 10.8 Hz might be a higher order vibration.

Fig. 5.4c compares the axial amplitude distributions for detector C and the resonances found at 9.9, 10.8 and 12 Hz. The curves for the two lower frequencies look very much alike and are most likely interpreted as higher order vibrations with fixed end conditions. As well as in the case for detector E, the 12 Hz resonance has a poor resolution. The idea that the 12 Hz resonance is a shift of the vibration at 10.8 Hz is still valid because the

5.1. Classification of Frequencies

12 Hz amplitudes are generally bigger and follow the trend of the curve at 10.8 Hz. It is assumed that the resonances at 9.9 and 10.8 Hz resemble higher order vibrations whereas the 10.8 Hz resonance is shifted to 12 Hz. The phenomenon of a shift in frequency was observed before but has not found an explanation yet. Unfortunately no publications could be found that discuss the occurrence of something like a shifted frequency.

Finally one has to judge the behavior of the curves created through the in-core measurement by detector D. The 9.9 Hz shape reminds of the shape of the fundamental mode whereas the 10.8 Hz shape reminds of the beam mode, cf. Fig. 5.4d. The maximum amplitude is found in the middle or in the lower part of the core, respectively, and classifying the vibrations apart from their fixed end conditions is not possible due to the lack of information from the literature.

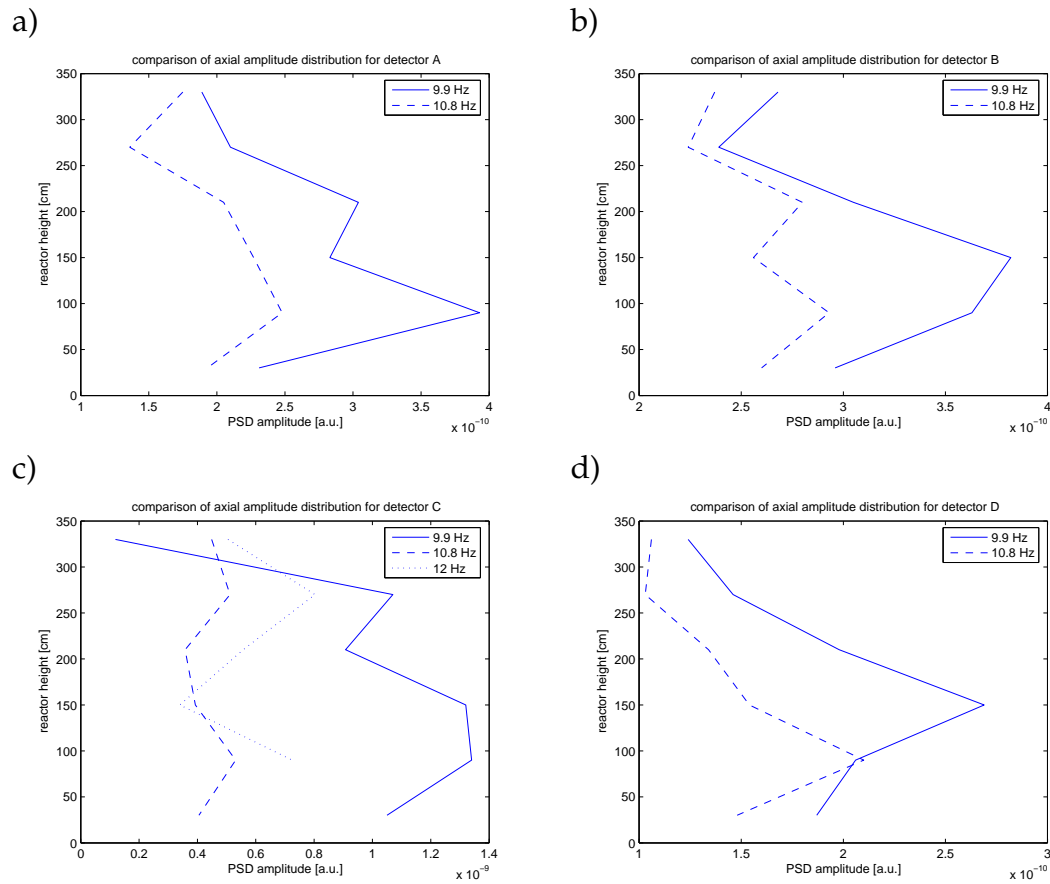


Figure 5.4: Comparison of the mode shapes in the range of 10 - 12 Hz for detectors A, B, C and D.

Chapter 5. Discussion and Conclusions

As a final conclusion here one can say that with the limited amount of measurement data and references it is impossible to fully classify the vibrations after their origin. Anyhow it is assumed that the resonances found at 9.9, 10.8 and 12 Hz are forced higher order vibrations of the fuel assemblies. The fuel assemblies furthermore might behave in various different manners due to mechanical properties or fuel content and radial fixings. The 15.5 Hz vibration could not even be classified as a real vibration and this is why it is neglected in the further consideration.

5.1.5 The Shell Mode - 19 Hz

From earlier works on the vibration modes of the core barrel it is well known that the shell mode vibration is found at about 20 Hz. As already mentioned in section 4.3 of the previous chapter, the resonance at 19 Hz could be measured in 40% of the signals, whereas only detector C allows plotting the axial amplitude distribution with a sufficient resolution. The shape observed in Fig. 4.7c does not apply to any of the theoretical mode shapes shown in the beginning of this chapter but since the amplitude has its maximum in the top of the core the vibration is assumed to have free conditions in the top and fixed conditions in the bottom.

5.1.6 The Pump Frequency - 24.9 Hz

When examining the shapes for the axial amplitude distribution of all 5 detectors at 24.9 Hz it becomes obvious that it is impossible to find any trend behavior. Detectors A and D are the only ones that have similar characteristics but C and E for example behave in an opposite manner.

One noticeable property of the resonance at 24.9 Hz observed in almost every spectrum was that the peak was particularly sharp and precise. Knowing that the revolution per minute of the pump that accelerates the primary coolant is 1500, one can easily conclude that the resonance at 25 Hz translates to a mechanical vibration caused by the pump frequency. It arises from the rotor blades that cause the coolant to flow upwards through the reactor core and is identified as the pump frequency.

CHAPTER 6

Summary

The in-core measurement at R4 used 5 in-core fission chambers at 6 axial positions to evaluate the mode shapes of the core and fuel vibrations. The purpose of this task was to find possible reasons for the unusual behavior of the reactor which was observed in earlier ex-core measurements. Since those results were of internal nature it was not possible to get hold of them. Analyzing the noise spectra obtained from the measurements made at R4 in 2008 via typical noise diagnostic methods led to the following results. The APSDs revealed 5 frequencies that could be classified after their type of vibration:

The top at 1.8 Hz could be found in a definite manner in 50 % of the measurements and was identified as the fundamental bending mode of the fuel assemblies.

It was found that the double peak in the 6 - 8 Hz range represents two different vibrations which unfortunately can be interpreted in two different manners.

The first interpretation states that the resonance at 6.8 Hz, which occurs in all measurement positions as a very strong peak, resembles the second bending mode of the fuel assemblies. At 7.8 Hz one finds that the APSD amplitude increases much in the lower part of the core, i.e. the vibrations here are stronger than in the upper part of the core. This behavior might originate from the pendulum movement of the core which also affects the core internals, hence the beam mode vibration can be observed with in-core instrumentation.

The second interpretation of the double peak is the contrary of the above. Previous in-core measurements at R4 (Karlsson, 1998) as well as the consideration of the analysis done in this work, cf. Fig. 4.6b, lead to the idea that the vibration at 6.8 Hz is caused by

Chapter 6. Summary

the pendulum movement of the core and, in turn, is interpreted as the beam mode vibration. This interpretation is intensified by considering the results of the three ex-core measurements done in the previous fuel cycle (Hernandez-Solis, 2008). Here it was observed that the higher resonance at around 8 Hz changed its value during the fuel cycle whereas the 6.8 Hz peak remained relatively constant. Generally it can be assumed that the beam mode vibration is more constant than the individual movement of fuel assemblies since they change their properties with time so that one could claim that the vibration at 7.9 Hz is associated with the eigenfrequency, or higher order bending mode, of the fuel assemblies which is induced by the coolant flow. This statement is again stressed by the results found in this, cf. Fig. 4.6c, and previous analyses. Furthermore one could see that the 6.8 Hz peak dominates over the 7.9 Hz peak when getting closer to the bottom of the core. This indicates that the beam mode vibration is stronger than the fuel assembly vibration with an own eigenfrequency which is a logical consequence when considering the construction of core and fuel assemblies.

In order to prove or disprove the interpretations made above additional measurements are necessary - so far, both ideas are just hypothetical.

Another resonance was found at 19 Hz. Even if this frequency was only measured in 40 % of the cases it could be identified as the shell mode vibration.

At 24.9 Hz, which is approximated to 25 Hz, the pump frequency was found.

Furthermore there are 2 forced vibration modes at 9.9 and 10.8 Hz where the latter one is assumed to be shifted to 12.8 Hz in the cases of detectors C and E. Detailed knowledge on those frequencies is not available yet but additional in-core measurements could help to analyze those resonances precisely and maybe even find their true origin.

The results obtained from this thesis can be corroborated by further in-core measurements. Unfortunately it was not possible to identify some of the vibrations more specifically, but additional noise diagnostics, also for the Ringhals reactor R3 which is similar in construction, would definitely improve the outcome of this thesis. As a final statement one can mention that noise diagnostics and the analysis of reactor vibrations is definitely a helpful tool to find typical core characteristics as well as probable anomalies. If there was not a lack of earlier measurement data and results it would

have been easier to assign those frequencies that have not found a specific explanation yet.

Chapter 6. Summary

Acknowledgements

It is difficult to know where to start since there were so many people involved in helping me on my journey so I hope that it is accepted if I start with the 3 people who mean the world to me.

Five years ago not even I believed that I will finish my studies, especially in physics, in the regular time. Studying was not always fun and definitely not easy but I am grateful that I stood out. Of course this would not have been possible without the unlimited support of my Mum and Dad. Therefore I thank my beloved parents first - without your love, trust and constant belief in me I could not have got through my life so far.

Secondly, I have to admit that Sweden as the choice for my foreign studies would have never been an option if I had not lost my heart to the "love of my life". After the two year long struggle of a relationship based on phone calls, e-mail and travelling between Germany and Sweden once every sixth week I was finally able to move to Gothenburg which I consider as "home!" today. Henrik, words cannot describe how much I love you and how thankful I am for letting me share my past, present and future with you.

A big "Thank you!" goes to Imre Pázsit for being the supervisor of this thesis and helping me with the difficult questions I had to face. Thanks for always making time for me and ending up in interesting discussions apart from physics.

Since the measurements were performed at the Ringhals Power Plant I would also like to thank Björn Severinsson, Martin Bengtsson, Tell Andersson and the staff behind the scenes for taking care of me and making this thesis possible.

Furthermore I send my regards to Anders Nordlund and Christophe Demazière for offering the education in Nuclear Engineering and being my lecturers. I am not sure whether my educational path would have guided me into the field of Nuclear Technique without the interesting course on "Reactor Physics" in the autumn term of 2006.

Thanks to my friend and roommate Katti as well as Davide, Augusto, Lennard and of course everyone else at the Department for Nuclear Engineering. I hope I do not have to leave you so soon!

Another very special thanks goes to Elisabeth Ericsson who helped me to fix all the paper work regarding me being a foreign student. Thank you for always giving me hope, acting quickly when I was in trouble with my course choice and being there when I just needed someone to talk to.

It is of course important to mention that I would have not gotten my scholarships without the help of Karin Robel and Jutta Wagler from the AAA at my home university BTU Cottbus.

And here we are back to where we started - in Cottbus. Big thanks to all my professors, lecturers and fellow students from BTU Cottbus. The three years of basic physics education were hard and sweaty but we had much fun together. I hope that I will have the chance to join you in the future when it is time for another "Paddeln & Grillen mit den Physikern".

Last but not least I have to thank all family members and friends - German and Swedish, old and new - who unfortunately find no name in this list of acknowledgements since I am running out of space: thank you for always being there when I need to escape from my routines!

WO WORTE NICHT AUSREICHEN

Nicht für den süßen Duft des feuchten Waldbodens
oder den wärmenden Sonnenstrahl, der meine Haut kitzelt;
nicht für den herrlich-salzigen Geschmack auf den Lippen nach einem
Spaziergang am Meer
oder den lieblichen Ton, der durch Musik erzeugt;
bin ich so dankbar, wie für das Erblicken des Glanzes in euren Augen, der
wortlos Liebe spricht.

Jede Sekunde seid ihr mit mir, bin ich mit euch
doch dieses eine Wort scheint viel zu klein
um allumschreibend für meine Gefühle zu sein:
(ich) LIEBE (euch)!

References

- Arzhanov, V., Pázsit, I. "Diagnostics of Core Barrel Vibrations by In-Core and Ex-Core Neutron Noise", 2003, *Progress in Nuclear Energy* 43, 151-158
- Demazière, C., Arzhanov, V., Karlsson, J. K.-H., Pázsit, I. "Final Report on the Research Project Ringhals Diagnostics and Monitoring, Stage 4", 1999, CTH-RF-145/RR-6
- Hernandez-Solis, A. "Diagnosis of centrifugal pumps", 2006 (Master Thesis), Department of Electrical Machines and Power Electronics, Royal Institute of Technology (KTH)
- Kim, H. K., Kim, M. S. "Vibration analysis of PWR fuel rod", 2005, *Journal of Sound and Vibration* 282, 553-572
- Kim, T.-R., Jung, S.-H., Park, J.-H., Choi, S. "Reactor Internals Vibration Monitoring in Korean Nuclear Power Plant", 1996, *Proceedings of a Specialists' Meeting on In-Core Instrumentation and Core Assessment*
<http://www.nea.fr/html/science/rsd/ic96/>, accessed 27.06.08
- Lamarsh, J. R. "Introduction to Nuclear Reactor Theory", 2002, American Nuclear Society
- Pázsit, I. "Transport Theory and Stochastic Processes", 2007 (lecture notes), Department of Nuclear Engineering, Chalmers University of Technology
- Pázsit, I., Kuang, Z. F., Prinja, A. K. "A unified theory of zero power and power reactor noise via backward master equations", 2002, *Annals of Nuclear Energy* 29, 169-170
- Pázsit, I., Demazière, C., Sunde, C., Hernandez-Solis, A., Bernitt, P. "Final Report on the Research Project Ringhals Diagnostics and Monitoring, Stage 12", 2008, CTH-RF-194/RR-14
- Smith, J. O. "Mathematics of the discrete Fourier Transform (DFT) with Audio Applications", 2007 (online book), Second Edition
<http://ccrma.stanford.edu/~jos/mdft/>, accessed 30.04.08

Sunde, C. "Noise Diagnostics of Stationary and Non-Stationary Reactor Processes", 2007 (PhD Thesis), Department of Nuclear Engineering, Chalmers University of Technology

Sunde, C., Wright, J., Demazière, C., Pázsit, I. "Final Report on the Research Project Ringhals Diagnostics and Monitoring, Stage 10", 2005, CTH-RF-194/RR-12, 30

Sweeney, F. J., March-Leuba, J., Wood, R. T. "Excitation Sources for Fuel Assembly Vibrations in a PWR", 1985, Transactions of the American Nuclear Society 49, 334-335

Thie, J. A. "Power Reactor Noise", 1981, American Nuclear Society

Tsoufanidis, N. "Measurement and Detection of Radiation", 1983, McGraw-Hill Book Company, 432-433

Weisstein, E. W. "Hanning Function" from MathWorld-A Wolfram Web Ressource

<http://mathworld.wolfram.com/HanningFunction.html>, accessed 29.04.08

Yun, W.-Y. "On-Line Vibration Monitoring of Core Support Barrel in Korean NPP", 2005 (ppt-presentation), IAEA Meeting on On-line Condition Monitoring of Equipment and Process in Nuclear Plants Using Advanced Diagnostic Systems

INTERNET-REFERENCES

www.barseback-kraft.net, accessed 16.06.08: "Technical Description of R4"

www.energimyndigheten.se, accessed 21.05.08: "Energy in Sweden Facts and Figures", 2007, Swedish Energy Agency

www.iaea.org, accessed 20.05.08: "Nuclear Technology Review 2007", 2007, International Atomic Energy Agency

www.mnf.co.jp, accessed 26.05.08

www.nndc.bnl.gov, accessed 15.06.08: "NNDC Database: ENDF", National Nuclear Data Center (Brookhaven National Laboratory)

www.nrc.gov, accessed 26.05.08: "Nuclear Reactors", U.S. Nuclear Regulatory Commission

www.vattenfall.com, accessed 20.05.08: "Ringhals Annual Report 2006", 2006, Vattenfall

www.westinghouse.com, accessed 26.05.08

www.world-nuclear.org, accessed 10.06.08: "Nuclear Power Information Papers Worldwide", World Nuclear Association